https://doi.org/10.5194/egusphere-2025-763
Preprint. Discussion started: 6 March 2025

Tracing the contribution of dust sources on deposition and phytoplankton carbon uptake in global oceans

Yaxin Liu [a], Yunting Xiao [a], Lehui Cui [a], Qinghao Guo [a], Yiyang Sun[a], Pingqing Fu[a], Cong-qiang Liu[a], Jialei Zhu [a, *]

[a] Institute of Surface-Earth System Science, School of Earth System Science, Tianjin University, Tianjin 300072, China

* Corresponding author.

Email address: zhujialei@tju.edu.cn

https://doi.org/10.5194/egusphere-2025-763
Preprint. Discussion started: 6 March 2025

ABSTRACT

Dust provides iron essential for marine phytoplankton growth, altering their carbon uptake capacity and affecting the global carbon cycle. However, due to the limited availability of observational parameters applied in evaluation models, there remains uncertainty in the contribution of marine dust deposition to carbon uptake. Here, we quantified the separate contributions of eleven major dust sources to dust deposition and marine ecological response to dust-borne iron in eight ocean regions based on the series of simulations constrained by multiple global observation datasets of iron solubility and total iron concentration in the oceans as well as iron content in the dust. Our simulations indicate that dust deposition could supply 11.1 Tg yr^{-1} of iron and 0.4 Tg yr^{-1} of dissolved iron to the oceans, promoting 5.6 Pg C yr^{-1} of carbon uptake by marine phytoplankton.

Keywords: Dust deposition; Carbon uptake; Fe supply; Source apportionment

https://doi.org/10.5194/egusphere-2025-763
Preprint. Discussion started: 6 March 2025

1 Introduction

Dust aerosol, the main component of atmospheric aerosols from arid and semi-arid areas, is the dominant exogenous input of Iron (Fe) to the surface of the ocean (Raiswell et al., 2012; Tagliabue et al., 2017). Dust carrying various micronutrients can be transported thousands of kilometers and deposited in remote ocean regions, ultimately resulting in the redistribution of nutrient elements (Jickells et al., 2005; Hamilton et al., 2022). Fe is an essential micronutrient for phytoplankton growth and can limit primary productivity in regions termed high nutrient, low chlorophyll (HNLC) regions, which comprise ~30% of the global ocean[5]. Several sources of Fe in the ocean have been identified, primarily including atmospheric dust, coastal inputs, and hydrothermal fluids (Tagliabue et al., 2017; Tagliabue et al., 2015; Boyd et al., 2010). When Fe enters the upper ocean, dFe is absorbed by marine organisms, such as phytoplankton and bacteria. After the organisms die, Fe is returned to the sediment, or, through physical processes, may be resuspended and re-enter the water column, completing the cycle (Boyd et al., 2010). However, Large amounts of fluvial and glacial particulate Fe are trapped in coastal areas (Poulton et al., 2002), and hydrothermal inputs are promptly precipitated at depth in the ocean. Therefore, dust is a major external source and dust deposition carrying Fe can promote photosynthesis and plankton growth, thereby impacting the carbon cycle and atmospheric carbon dioxide (CO_2) (Mahowald et al., 2011; Johnson et al., 2013; Kanakidou et al., 2018; Pavia et al., 2020; Westberry et al., 2023). Nevertheless, quantitative assessments of the linkage between dust sources and their effects on marine biogeochemical cycles in various

https://doi.org/10.5194/egusphere-2025-763
Preprint. Discussion started: 6 March 2025

oceanic regions are still lacking (Shoenfelt et al., 2019; Hamilton et al., 2023).

One key reason current studies struggle to estimate marine carbon uptake to dust-borne Fe is the uncertainties in assessing the dissolved Fe (dFe) (Hamilton et al., 2023). Changes in the supply of dFe within its range of uncertainty can lead to substantial differences in carbon uptake (Dietze et al., 2017; Watson et al., 2000; Spolaor et al., 2013), since only dFe can be utilized by phytoplankton instead of all Fe in deposited dust (Mahowald et al., 2005; Shaked et al., 2005). Thus, accurately evaluating the dFe supply from dust deposition over the ocean is vital to assessing the carbon uptake caused by dust. The Fe content in dust and solubility of dust-borne Fe vary among different dust source regions (Struve et al., 2022). Therefore, determining the contributions of dust source regions to various oceans separately is essential for accurately assessing the dust-borne dFe. Previous studies have predominantly focused on investigating the spatiotemporal variations of global or regional dust emissions (Choobari et al., 2014; Wang et al., 2014; Ginoux et al., 2001; Mahowald et al., 2003; Tegen et al., 2004), as well as the dust deposition fluxes to oceans (Zheng et al., 2016; Kok et al., 2021). Some studies evaluated global Fe cycle and Fe deposition using models (Myriokefalitakis et al., 2015; Zhang et al., 2015). However, the specific dust and Fe contributions of the various dust sources to the distinct oceans remain insufficiently understood, hindering a systematic understanding of the Fe supply relationships between sources and oceans, as well as their seasonal variations and underlying mechanisms. Moreover, dust usually undergoes complex atmospheric chemical processes during long distance transport, resulting in enhanced solubility of

https://doi.org/10.5194/egusphere-2025-763
Preprint. Discussion started: 6 March 2025

Fe within the dust particles (Longo et al., 2016; Li et al., 2017; Félix-Bermúdez et al., 2020; Kurisu et al., 2024). Consequently, the dFe content in dust transported to remote oceanic regions is typically higher than that in dust from the sources (Shi et al., 2012). The content of total Fe in aerosols can vary by a factor of 2 (Mahowald et al., 2005; Mahowald et al., 2011). Due to the complexity and uncertainty of atmospheric chemical processes including acidic reactions and photoreduction, accurately simulating the dFe content in dust deposited in remote oceanic regions is challenging. In previous studies, the Fe content of deposited dust is usually assumed to be 3.5%, while its solubility is assumed to be 2% (Jickells et al., 2005; Hamilton et al., 2022; Mahowald et al., 2005; Mahowald et al., 2017), overlooking their variability in different sources and chemical processes during transport. This assumption may lead to uncertainties in evaluating the Fe deposition from dust sources and the input of Fe to the oceans.

The struggle to accurately quantify the relationship between Fe availability and carbon uptake is a key problem limiting the evaluation of the marine carbon uptake to dust-borne input of Fe. Previous studies have verified that dust-borne inputs of Fe can enhance the carbon uptake, thereby impacting the carbon cycle (Bishop et al., 2002; Patra et al., 2007; Ziegler et al., 2013; Kobayashi et al., 2021). The large decline in atmospheric CO_2 during past glacial periods coincided with an increase in observed Southern Ocean marine productivity and substantial dust deposition as recorded in marine sediments and ice cores (Ziegler et al., 2013; Lambert et al., 2008; Wolff et al., 2010). Model simulations also indicate that the Fe fertilization from glaciogenic dust played an important role in enhancing carbon storage and declining atmospheric CO_2

https://doi.org/10.5194/egusphere-2025-763
Preprint. Discussion started: 6 March 2025

concentration (pCO_2) (Kobayashi et al., 2021). However, quantifying the carbon uptake caused by dust-borne inputs of Fe remains highly uncertain due to the complex processes during dust transport and the difficulty in quantifying phytoplankton growth induced by Fe supply from dust deposition. Gao et al (2001) estimated Fe deposition over the global ocean based on in situ observations and proposed that using satellites for similar research is feasible in the future soon. However, satellite data cannot reliably quantify the linkage between Fe fluxes and phytoplankton biomass and productivity on a global scale due to obstacles. These include the inability to provide accurate flux measurements of aerosols reaching the ocean surface at designated locations and pervasive cloudiness that disrupts observations of high-latitude oceans. These factors prevent satellite data from being a reliable method to quantify the linkage between Fe fluxes and phytoplankton biomass and productivity on a global scale (Hamilton et al., 2023). Several studies have tried to quantify the responses of marine biogeochemistry to dust deposition on large scales based on model simulations and observations (Mahowald et al., 2009; Mahowald et al., 2010; Ito et al., 2020), but the results vary largely due to the different global parameterization models. Given the complex and dynamic environmental conditions experienced by phytoplankton growth in the ocean, the ratios of carbon to nutrients in exported organic matter have long been used to simplify biogeochemical cycles (Twining et al., 2015; Wiseman et al., 2023). Ratios, such as Fe to carbon (Fe: C) ratios for new growth, help determine the efficiency of the biological export of carbon (Wiseman et al., 2023). In HNLC regions, Fe is the main limiting factor inducing phytoplankton blooms, and consequently influencing carbon

https://doi.org/10.5194/egusphere-2025-763
Preprint. Discussion started: 6 March 2025

uptake (Matrin et al., 1990; Boyd et al., 2007). In low nutrient, low chlorophyll (LNLC) regions, Fe can also alleviate nutrient-limiting pressure, and dust addition can stimulate nitrogen fixation, thereby promote phytoplankton growth and impacting the carbon cycle (Zhang et al., 2019; Okin et al., 2011; Mills et al., 2004). Therefore, Fe is a significant limiting nutrient over global oceans, and Fe: C ratios by phytoplankton could be considered as a bridge to estimate the global marine carbon uptake to dust deposition. Wiseman et al (2023) proposed a clearly dynamic relationship between phytoplankton Fe: C ratios and ambient dFe concentrations, making it possible to quantify the variations of marine carbon uptake caused by dust-borne inputs of dFe which could provides integrated insights into past climatic events and aids future marine-based CO_2 removal initiatives for climate mitigation.

In this study, we conducted a series of sensitivity experiments using the Community Earth System Model (CESM) to apportion the contributions of various dust sources to dust deposition and Fe supply in different marine areas globally. By incorporating the Fe content of dust from diverse source as well as observations of oceanic Fe solubility and content from numerous sites, we calculated the carbon uptake by phytoplankton resulting from dust deposition in various marine areas. This research employs an observation-driven approach, providing a new perspective for assessing the impact of dust on the global carbon cycle and attempting to establish a more accurate and detailed link between different dust sources and carbon uptake by phytoplankton in various marine areas.

https://doi.org/10.5194/egusphere-2025-763
Preprint. Discussion started: 6 March 2025

2 Methods

2.1 Community Earth System Model

CESM version 1.2.2 (Hurrell et al., 2013) is employed in this study, which is a community tool to figure out the behavior of Earth's climate. In the model, atmospheric dust is emitted from the land by wind in the Community Land Model (CLM) (Mahowald et al., 2006). The wind friction speed, vegetation cover, and soil moisture are key factors which could determine the soil erodibility and dust emission. The dust emission scheme employed into CLM based on the Dust Entrainment and Deposition (DEAD) model of Zender et al (2003). More details could be found in Technical Description of CLM v4.0 (Oleson et al., 2010).

In dust model, the total vertical dust mass flux (F_j, kg m^{-2} s^{-1}), from the ground into transport bin j is calculated by the following function:

$$F_j = TSf_m\alpha Q_S \sum_{i=1}^{I} M_{i,j} \quad (1)$$

Where T is a tuning factor, S is the source erodibility which likes a place holder, f_m is the grid cell fraction of exposed bare soil, α is the sandblasting mass efficiency (m^{-1}), Q_S is the total horizontally saltating mass flux (kg m^{-1} s^{-1}), and $M_{i,j}$ is the mass fraction of each source mode i carried in different bin j.

2.2 Regions classification and sensitivity experiments

To identify the contributions of dust source regions to the oceans, eleven main dust source regions and eight ocean regions were classified. Most dust is emitted from the so-called "dust belt", which includes northern Africa, the Middle East, central Asia, and the northwest of China and the Mongolian deserts. Small amounts of dust are emitted

https://doi.org/10.5194/egusphere-2025-763
Preprint. Discussion started: 6 March 2025

from Australia, southern Africa, and North and South America. In addition to considering the primary dust sources, the varying iron content of the dust is also a factor in defining the dust source regions. Ultimately, we divided dust sources over the world into eleven source regions that together account for the overwhelming total of desert dust emissions identified in models. Eleven dust source regions are Northwest Africa (NWAf), Northeast Africa (NEAf), Middle Africa (MAf), South Africa (SAf), North America (NAm), South America (SAm), West Asia (WAs), Middle-North Asia (MNAs), East Asia (EAs), South Asia (SAs), and Australia (AU), respectively. The apportionment of the source regions partially follows the definition provided by Kok et al (2021), with the main difference being that we divided Asia into more regions due to variations in iron content.

30°S and 30°N are the boundaries for dividing the difference ocean regions. The north of 30°N is North Pacific Ocean (NP), North Atlantic Ocean (NA), Mediterranean Sea (MS), respectively. The south of 30°S is Southern Ocean (SO), In addition, between the 30°N and 30°S is Equatorial Pacific Ocean (EP), Equatorial Atlantic Ocean (EA), Equatorial Indian Ocean (EI), respectively. In total, eleven dust source regions corresponding with eight deposit ocean regions are classified in this study as shown in Fig. 1.

Given that Fe is the primary limiting nutrient in HNLC regions, we calculated the marine carbon uptake for new growth attributable to dust deposition in these regions. Three main HNLC regions as selected and defined by Aumont et al (2006) include the Southern Ocean (SO) south of 40°S, the equatorial Pacific (EP) between 5°S - 5°N and

https://doi.org/10.5194/egusphere-2025-763
Preprint. Discussion started: 6 March 2025

180°W - 80°W, and the subarctic North Pacific (NP) north of 40°N and spanning 140° E - 120°W (Fig. 1).

We ran the baseline case with global dust emissions. In each experimental case, emissions from a specific dust source region were turned off, and the difference between this scenario and the baseline case was considered as the dust emission and deposition from that particular dust source region. We ran five years simulation for investigating the long-term characteristics of global dust emission and ocean deposition, and all the simulations were run with a spin-up for one year.

2.3 Fe Solubility and dissolved Fe concentration data

To accurately estimating the Fe supply to the ocean from dust deposition, we used varying Fe content data for different dust source regions based on ten-year-averaged percentages of elements over desert regions provided in Zhang et al (2015). The Fe contents in NWAf, MAf, NEAf, SAf, NAm, SAm, WAs, MNAs, EAs, SAs and AU are 2.00%, 2.65%, 1.91%, 2.47%, 2.38%, 2.28%, 2.20%, 1.76%, 2.08%, 2.17% and 2.70%, respectively.

Fe solubility is also a key factor to estimate the carbon uptake of ocean to dust deposition. Since the complex particle-aging processes during dust transport would influence the solubility of dust-born Fe (Longo et al., 2016), the observed Fe solubility in different oceans were used to constrain the Fe solubility in specific marine areas. The observation data, introduced in Ito et al (2019), included 774 sites of Fe solubility across various oceans. To mitigate the risk of overestimating the contribution of dust-borne Fe, Fe solubility data were filtered to retain only values below 6.0%, based on the studies

https://doi.org/10.5194/egusphere-2025-763
Preprint. Discussion started: 6 March 2025

by Shi et al (2011a), Shi et al (2009), Shi et al (2011b), Journet et al (2008), Tapp et al (2010) and Scanza et al (2018). Shi et al (2011) found that Fe solubility ranged from approximately 0.1% to 0.8% in various size fractions of Saharan soil samples. After cloud processing, Fe solubility of Saharan soil sample could increase to 3.5% (Shi et al., 2009). Shi et al (2011b) measured potential Fe solubility of Saharan soil dust samples approaching 6%. However, Fe solubility of dust could increase during transport, which is attributed to the complex atmospheric chemical processes, including acidic reactions and photoreduction (Longo et al., 2016; Li et al., 2017). Journet et al (2008) and Trapp et al (2010) found maximum solubility values of 5.25% and 5.8%, respectively, by measuring African dust collected over the Atlantic Ocean, Mediterranean Sea, and Barbados, which had experienced atmospheric transport. Consequently, we filtered the Fe solubility data to retain only values below 6.0%. Since the Fe solubility data used in this study are derived from multiple sources, not solely from dust, there is a possibility that the filtered-out Fe solubility data may be overestimated if regarded as representative of dust, as these data could originate from other sources, such as combustion. Scanza et al (2018) showed that the global Fe solubility from both dust and combustion sources, as simulated, ranged from 0% to 20%. Ultimately, 514 data points were retained and interpolated to a resolution of 1.9° ×2.5° for this study. The mean Fe solubility interpolated from observations is 2.8%, which is comparable to the assumed value of dust Fe solubility (2%) by previous studies[3], but incorporates spatial distribution (Fig. S1).

The dFe concentration data is a necessary factor for calculating the Fe: C ratio.

https://doi.org/10.5194/egusphere-2025-763
Preprint. Discussion started: 6 March 2025

The dFe concentration data used in this study is from the GEOTRACES Intermediate Data Product 2021 Version 2 (https://www.bodc.ac.uk/geotraces/data/idp2021/). GEOTRACES is an international study of the marine biogeochemical cycles of trace elements and isotopes, and provides a broad coverage of observational data on aerosol nutrients (Schlitzer et al., 2018). A total of 15970 data of dFe concentration across 3304 sites over ocean were obtained. Data overlapping on the same sites were averaged, and the resulting observed dFe concentration over ocean were interpolated into a resolution of 1.9°×2.5° for this study (Fig. S2).

2.4 Inverse distance weighting interpolation

We employed the inverse distance weighting (IDW) method, a widely used spatial interpolation technique, to interpolate observation data on Fe solubility and dFe concentration to a resolution of 1.9°×2.5°. The globe was divided into a grid matrix of 144×96 cells based on simulation results from CESM. Observations were matched to the grid matrix using spatial coordinates and subsequently interpolated using the IDW method. Spatial distances between each interpolation grid and observation locations were calculated iteratively. Weight functions were then applied to these distances to compute a weighted average, yielding the interpolated results.

The function to calculate the weight is as follows:

$$w_i = \frac{1}{d_i^P} \quad (2)$$

Here, w_i represents the weight of the i-th observation, d_i is the distance between the observation location and the interpolation point, and P is a tuning factor set to 3 for this interpolation.

https://doi.org/10.5194/egusphere-2025-763
Preprint. Discussion started: 6 March 2025

The weights are applied to calculate a weighted average, yielding the interpolated results. The formula for calculating the weighted average is expressed as follows:

$$z(x,y) = \frac{\Sigma_{i=1}^{N} w_i z_i}{\sum_{i=1}^{N} w_i} \quad (3)$$

Here, $z(x,y)$ is the interpolated result, N is the number of the observations, (x,y) denotes the coordinates of the i-th observation, w_i is its weight, and z_i is the observed data.

2.5 Calculation of Carbon Uptake

The contribution of each dust source region to the dissolved iron deposition in various marine areas can be calculated based on dust deposition rates and iron solubility. Then, Fe: C ratios are employed to calculate carbon uptake caused by dust deposition with the function as follows:

$$C = \frac{D * Fe_{con} * Fe_{sol}}{gQfe} \quad (4)$$

where C is the amount of marine carbon uptake driven by dust deposition, D is the amount of dust from source regions and deposit to oceans, Fe_{con} is the Fe content for different dust source region, and Fe_{sol} is the solubility of Fe over various oceans.

Phytoplankton Fe: C ratio for new growth (gQfe) is defined to be a linear function of the ambient soluble Fe concentration in specific marine area (Sunda, 1995), which is a vital link for estimating the marine carbon uptake to variations of dust-borne inputs of Fe. The following is the function to calculate Fe: C ratio used in this study (Wiseman et al., 2023):

$$gQfe = \min\left(gQfe\_max,\ \max\left(gQfe\_min, gQfe\_max \times \frac{dFe}{FeOpt}\right)\right) \quad (5)$$

where gQfe is the Fe: C ratio for new growth, gQfe_max is the prescribed

https://doi.org/10.5194/egusphere-2025-763
Preprint. Discussion started: 6 March 2025

maximum Fe: C, gQfe_min is the prescribed minimum Fe: C, dFe is the local concentration of soluble Fe, and FeOpt is the iron concentration where Fe: C ratio reaches its maximum value. In this study, we used a broad Fe: C ratio range for new growth (3-90 μmol Fe mol^{-1} C) and an FeOpt of 1.75 nM for all phytoplankton groups which are proposed by Wiseman et al (2023).

3 Results

3.1 Spatial and temporal characteristics of global dust emission and deposition over the oceans

Our simulations indicate a global annual average dust emission of 2071.5 Tg (Fig. 2). The highest dust emission concentrated in North Africa (i.e. NEAf and NWAf), surrounding the Sahara Desert. Dust emission from NEAf and NWAf accounts for 58.0% of global dust emission, with NEAf exhibiting a stronger intensity of dust emission compared to NWAf. Dust emitted from WAs (317.7 Tg yr^{-1}) is also a key contributor to global dust emission, accounting for 15.3% of global dust emission. The northeastern region of the Arabian Desert, located on the Arabian Peninsula, is the primary area of dust emission within WAs, while the east of the Caspian Sea is also notable for its strong dust emissions, attributed to the presence of the Kyzylkum Desert and Karakum Desert (Fig. 2). Furthermore, the SAs and EAs regions are also high emission sources, including the Taklamakan Desert, Gobi Desert, and several small deserts such as the Badain Jaran Desert, Tengger Desert, Ulan Buh Desert, and Kubuchi Desert. Dust emissions from SAf, America (NAm, SAm), and MNAs are minor contributors to global dust emissions, each accounting for ~1% of the total dust emission. The

https://doi.org/10.5194/egusphere-2025-763
Preprint. Discussion started: 6 March 2025

contributions of the main dust sources to global dust emissions in this study are comparable with the results presented by Jickells et al (2005) and Wang et al (2024).

Global dust emissions exhibit large seasonal variations, with emissions during spring and summer (663.0 and 667.1 Tg season^{-1}) being approximately 70-90% higher than those in autumn and winter (349.3 and 392.2 Tg season^{-1}) (Fig. S3). This is largely attributed to the pronounced seasonal variations in dust emissions from the Asian region (Fig.S3 and 3). Dust emissions in EAs and SAs during spring (67.2 and 94.7 Tg) are 813.6% and 436.2% higher than those in winter (7.4 and 17.7 Tg) in EAs and SAs, respectively. During winter, surface temperatures in SAs and EAs can drop to below -30°C, leading to soil freezing and reduced dust emissions (Fig. S4). The seasonal variations of dust emission in the Southern Hemisphere, such as SAf, SAm and AU, are similar. In these areas, dust emissions peak in autumn with SAf, SAm, and AU emitting 10.0, 3.6 and 26.6 Tg, respectively. In comparison, spring is the season with low dust emission season in these regions (3.21, 1.38 and 11.2 Tg) (Fig.3).

There are 560.2 Tg dust deposited into ocean every year (Fig. 4), representing 27.0% of the annual global dust emission. Wet deposition dominates the dust deposition, accounting for 77.4% of the total dust deposition to the ocean (Fig. 5). As shown in Fig. 4, the dust deposition over EA (235.0 Tg yr^{-1}) and EI (132.9 Tg yr^{-1}) is highest among oceans around the world. Dust depositions in the EP, NP, MS, RS and SO regions show a decreasing trend, with annual dust deposition of 53.8, 46.0, 28.2, 26.2 and 19.1 and 18.9 Tg, respectively. NA has the lowest dust deposition of 18.9 Tg yr^{-1}, indicating that northwestward transport is not the primary direction for dust from Africa. In addition,

https://doi.org/10.5194/egusphere-2025-763
Preprint. Discussion started: 6 March 2025

the contributions of dry deposition to dust deposition in all oceans are generally less than 30%, much lower than that of wet deposition, except in the RS and MS. The proportions of dry deposition in RS and MS are 52.0% and 46.4%, respectively, due to their relatively small areas with low precipitation and proximity to dust sources.

Global marine dust deposition in summer (209.4 Tg season^{-1}) is higher than other seasons (Fig. S5) (147.5 Tg season^{-1} in spring, 96.8 Tg season^{-1} in autumn and 106.5 Tg season^{-1} in winter). In summer, dust deposition in EI increases sharply, rising by 337.6% compared to spring, primarily due to the increase of wet deposition (Fig. S6 and S7). The large reduction in dust deposition in EA during autumn, which is ~60 Tg lower than in other seasons, is the primary reason for the lowest global dust deposition during this period. As EA is a key source of marine dust deposition, this sharp decline in autumn emissions is a major contributor to the global decrease in dust deposition. (Fig. 6). Generally, high dust deposition occurs in spring and summer, while low dust deposition occurs in autumn and winter in all oceans except for SO and MS. (Fig. 6). Dust deposition in SO peaks in autumn, while it is lowest in the spring (Fig. 6). The MS experiences its lowest dust deposition in summer, with 3.3 Tg, a pattern that contrasts with the higher summer deposition seen in other oceanic regions. Moreover, seasonal variations of dust deposition are drastic in RS, EI and NP with changes of 626.1%, 600.4% and 550.0%, respectively.

3.2 Annual and seasonal contributions of dust sources to deposition over ocean

The source apportionment of dust deposition over eight oceans were conducted through a series of sensitivity experiments. Dust from NWAf and NEAf are the major

https://doi.org/10.5194/egusphere-2025-763
Preprint. Discussion started: 6 March 2025

contributors to dust deposition over EA, NA, MS and EP, accounting for more than 50% of dust deposition in each of these oceans (Fig. 7). Dust from NEAf is also the dominant contributor to dust deposition over RS, while dust from NWAf makes only a minor contribution due to a small portion of dust from NWAf being transported eastward (Fig. 7). EA is the ocean with the highest dust deposition over the world, which is primarily attributed to the dust transported westward from NWAf and NEAf. Dust from NWAf (46.0%) contributes slightly more to deposition over EA than dust from NEAf (44.2%), as a greater amount of dust from NWAf can be westward transported to EA than from NEAf (Fig. 7).

EI is the ocean with the second highest dust deposition, primarily due to the overwhelming southward transport of dust from WAs, accounting for 59.1% (Fig. 7). The second largest contributor to dust deposition over EI is dust from NEAf, accounting for 22.7%, mainly owing to the primary eastward transport from NEAf. The following contributor to EI's dust deposition is dust from SAs, accounting for 10.0% (Fig. 7). Dust deposition in other oceans is comparatively lower than that in the EA and EI regions, but each with distinct source characteristics. EP and NP have similar dust deposition, accounting for 9.6% and 8.2% of total dust deposition over global oceans, respectively, but their major contributors are quite different. The major contributors to dust deposition over EP are NWAf and NEAf, while they are EAs and SAs for NP (Fig. 7). Moreover, dust deposition over NP is mainly from Asia except for MNAs, while dust from MNAs is primarily deposited over EP (Fig. 7). Dust deposition over MS and RS is similar (29.5 and 26.2 Tg yr^{-1}), accounting for 5.3% and 4.7% of total dust

https://doi.org/10.5194/egusphere-2025-763
Preprint. Discussion started: 6 March 2025

deposition over the ocean, respectively. Dust from NEAf and NWAf dominate the dust deposition over MS, accounting for 98.6%. However, NEAf is the primary contributor to dust deposition over RS, while dust from NWAf contributes little (Fig. 7). Additionally, dust deposition over SO is mainly from dust sources in the Southern Hemisphere (i.e. AU, SAf, and SAm).

As mentioned above, the largest global marine dust deposition occurs in summer dominated by the large dust deposition over EI in summer (Fig. S5). The seasonal variations in contributions from dust sources to oceans further explain this increase in summer. The primary contributor to dust deposition over EI is dust from WAs, which primarily transports southward and deposits over EI through the year (Fig. 8). In summer, dust emission from WAs peaks with the highest ratio of deposition to emission in WAs, which is 20% higher (up to 47.4%) than in other seasons (Fig. 3 and S3). The proportion of dust from WAs deposited over EI in summer (85.3%) is 10-30% higher than in other seasons (Fig. 8). In addition, dust from NEAf is predominantly transported eastward in summer, leading to an increase of ~30% compared to other seasons in the amount of dust from NEAf deposited over EI (Fig. 8). Dust emission from NEAf is also highest in summer, with the ratio of deposition to emission slightly higher by ~7% than in other seasons. Therefore, dust deposition over EI in summer is six times higher than in other seasons.

The dust deposition over EA in autumn is 29.4% lower than that in other seasons (Fig. 6). Dust from NWAf and NEAf are consistent major sources of dust deposition over EA, contributing ~90% of the dust deposition to EA through the year (Fig. 8). Dust

https://doi.org/10.5194/egusphere-2025-763
Preprint. Discussion started: 6 March 2025

emissions from NWAf and NEAf are 59.1% and 45.7% lower in autumn compared to their peak seasons (spring for NWAf and summer for NEAf) (Fig. 3). Therefore, the decrease in dust deposition over EA in autumn is primarily due to reduced dust emissions from these two key contributors.

The lowest amount of dust deposition over oceans typically occurs in autumn and winter, except for MS, where it occurs in summer (Fig. 6). Dust from NWAf and NEAf are consistently accounts for more than 98% of total dust deposition over MS as major contributors (Fig. 8). However, in summer, less dust from NWAf and NEAf is transported and deposited over MS, decreasing by ~10% and ~6%, respectively, compared to other seasons.

Dust deposition over RS, EI, NP and EP exhibits the largest seasonal variations among ocean areas, with variations of 626.3%, 600.4%, 550.0% and 424.9%, respectively. NEAf and WAs have consistently been the primary sources of dust deposition in the RS region, contributing over 90% of the total, though their respective contributions show noticeable seasonal variations (Fig. 8). During the summer, the eastward transport of dust from NEAf increases, leading to a 15-21% rise in its contribution to dust deposition in the RS region compared to other seasons (Fig. 8). The contribution of dust from NEAf shows a significant increase only in summer, further widening the gap with seasons of lower dust deposition. This is a key factor in the 626.3% increase in dust deposition over the RS in summer compared to winter (Fig. 6). The seasonal variation in dust deposition over the NP region is driven by the large seasonal variations in Asian dust emissions as its primary source (Fig. 8). Dust from EAs and

https://doi.org/10.5194/egusphere-2025-763
Preprint. Discussion started: 6 March 2025

SAs consistently contributing over 80% of the dust deposition over the NP area with emission peak in spring (Fig. 8). As a result, dust deposition over NP is much higher in spring than in other seasons, with an increase of 550.0% compared to winter. The primary sources of dust deposition over EP are also dust sources in Asian, except during summer (Fig. 8). The primary contributors to dust deposition over EP in summer are NWAf and NEAf, accounting for 73.0% (41.6% for NWAf and 31.4% for NEAf). Dust from NWAf and NEAf leads to 2 to 26 times more dust deposition over the EP during the summer compared to other seasons, resulting in a large seasonal disparity in dust deposition. Therefore, dust deposition over EP in summer is 424.9% higher than that in winter.

3.3 Spatiotemporal patterns in carbon uptake for new growth driven by dust-borne iron supply

According to the function (4), the Fe: C ratio is a crucial factor in calculating carbon uptake for new growth induced by dust deposition into the ocean. We utilize a dataset of Fe: C ratios derived from observations (Ito et al., 2019; GEOTRACES Intermediate Data Product Group, 2023) to the same grid as our simulations. A small Fe: C ratio indicates large carbon uptake for new growth driven by the same amount of Fe supply. Increased Fe supply usually can enhance carbon uptake by phytoplankton, but only soluble Fe is bioavailable, making the solubility of Fe key to the marine's carbon uptake for new growth to dust deposition. Thus, we incorporate varying Fe contents for each dust source and utilize a dataset of Fe solubility to the same grid based on observations (Zhang et al., 2015; Ito et al., 2019). The interpolated result of Fe solubility showed high Fe solubility was primarily occurred in EA and NA, particularly

https://doi.org/10.5194/egusphere-2025-763
Preprint. Discussion started: 6 March 2025

in north-central EA. Relatively high Fe solubility was also found in the regions spanning 105°W-130°W and 45°E-75°E in the SO (Fig. S1). The amount of dust deposition is fundamental in determining the marine carbon uptake for new growth to Fe supply from dust. Consequently, the relationship between dust deposition in various oceans and their respective dust sources elucidates the link between carbon uptake for new growth in each marine region and its dust sources. We estimated the global marine carbon uptake associated with new growth resulting from dust deposition, using the Fe:C ratio, since, regardless of whether in HNLC or LNLC regions, phytoplankton can respond to dust deposition. However, Fe is not the sole primary limiting nutrient in LNLC regions; therefore, we also quantified the marine carbon uptake resulting from new growth driven by dust deposition exclusively in HNLC regions.

Our simulations indicate that annual dust deposition supplies 11.1 Tg of Fe to the ocean, of which 0.4 Tg is dFe, driving a carbon uptake of 5.6 Pg C yr^{-1} by phytoplankton. High dust-borne dFe primarily occurs in EI (1.1×10^{-1} Tg yr^{-1}), EA (1.7×10^{-1} Tg yr^{-1}), and MS (1.7×10^{-2} Tg yr^{-1}) (Fig. S8). The high Fe: C ratio is primarily occurred in EA, particularly in the north-central of EA (Fig. S9). The mean Fe: C ratio in EA is the highest, which is 62.5 μmol Fe mol^{-1} C. The NP and EP near America, as well as NA, exhibit relatively high Fe: C ratios (Fig. S9). The average Fe: C ratios in NP, EP, and NA are 19.6, 27.6, and 28.0 μmol Fe mol^{-1} C, respectively. Large carbon uptake driven by dust deposition occurs primarily in EA, EI and RS (Fig. 9), which exhibit positive ecological responses to dust deposition, with uptake values of 2.3, 1.7 and 0.5 Pg C yr^{-1}, respectively. The following areas are NP (0.4 Pg C yr^{-1}), EP (0.3 Pg C yr^{-1}), NA (0.2

https://doi.org/10.5194/egusphere-2025-763
Preprint. Discussion started: 6 March 2025

Pg C yr^{-1}) and MS (0.2 Pg C yr^{-1}). The carbon uptake for new growth driven by dust deposition is minimal in the SO (0.1 Pg C yr^{-1}), accounting for only ~3% of the total carbon uptake for new growth driven by global dust deposition. The spatial distribution of carbon uptake for new growth driven by dust deposition closely mirrors that of dust deposition. In EA, carbon uptake for new growth driven by dust deposition decreases from east to west, while in EI, the northwestward region exhibits high values (Fig. 9). Despite the large Fe: C ratio in EA, which means the carbon uptake for new growth by phytoplankton is not sensitive to dust-born Fe supply, it remains the region with the largest carbon uptake for new growth to dust deposition, accounting for 41.3% of the marine carbon uptake for new growth induced by dust deposition (Fig. 9 and S9). This strong response is supported by the highest Fe supply from dust deposition (4.7 Tg yr^{-1}) and Fe solubility (6.7% in average) in EA. The intensity of carbon uptake for new growth driven by dust deposition in RS is much higher than that in other oceans, mainly because of the lowest Fe: C ratio in RS (7.0 μmol Fe mol^{-1} C) (Fig. 9 and S9). In addition, compared to the role in global dust deposition over the oceans, the contributions of carbon uptake for new growth driven by dust deposition in EP is smaller due to low Fe solubility (1.9%) and high Fe: C (27.6 μmol Fe mol^{-1} C).

The global marine carbon uptake for new growth driven by dust deposition in summer is 2.1 Pg C $season^{-1}$ while that is ~1.0 Pg C in other seasons (1.4 Pg C $season^{-1}$in spring, 0.9 Pg C $season^{-1}$ in autumn and 1.2 Pg C $season^{-1}$in winter) (Fig. 10). During summer, phytoplankton in EI, EA and RS contribute most to the global marine carbon uptake induced by dust deposition, with EI at 0.9 Pg C, EA at 0.5 Pg C and RS at 0.3

https://doi.org/10.5194/egusphere-2025-763
Preprint. Discussion started: 6 March 2025

Pg C, in addition, the carbon uptake for new growth over EI and RS are much higher in summer than other seasons (Fig. 11). Except for summer, EA has the largest marine carbon uptake for new growth driven by dust deposition among all ocean areas (Fig. 11). Generally, high carbon uptake for new growth usually occurred in spring and summer, and low carbon uptake for new growth occurred in autumn and winter, in addition to SO, MS and EA (Fig. 11). The seasonal variations of carbon uptake for new growth in SO and MS are dominated by the seasonal variation in dust deposition. Nevertheless, the seasonal changes in carbon uptake for new growth in EA differ from the seasonal pattern of its dust deposition. High carbon uptake for new growth in EA occurs in winter (0.7 Pg C) and spring (0.7 Pg C), while low carbon uptake for new growth occurs in autumn (0.4 Pg C) and summer (0.5 Pg C) (Fig. 11). In comparison, high dust deposition in EA occurs in spring (65.67 Tg), winter (61.8 Tg) and summer (61.2 Tg), the lowest dust deposition occurs in autumn (46.4 Tg) (Fig. 6). These differences are mainly due to the difference in the seasonal pattern between Fe: C ratio and dust deposition in EA. The seasonal variations and spatial distribution of carbon uptake for new growth in the EA region are largely influenced by the Fe: C ratio, in addition to the impact of dust deposition. High carbon uptake for new growth in EA during winter and spring is mainly distributed in the middle region, where Fe: C ratios are relatively low (Fig. S9). In contrast, during autumn and summer, high carbon uptake for new growth is centered in the northern EA, where Fe: C ratios are high (Fig. S9).

Since Fe is the most primary limiting factor in HNLC regions, we estimated the result of marine carbon uptake for new growth induced by dust deposition only over

https://doi.org/10.5194/egusphere-2025-763
Preprint. Discussion started: 6 March 2025

HNLC regions. The results show that annual dust deposition provides 0.8 Tg Fe to HNLC regions, of which 2.2×10^{-2} Tg is dFe, causing a marine carbon uptake of 0.2 Pg C yr^{-1} for new growth. The carbon uptake for new growth driven by dust deposition occurred in the HNLC region over NP, SO and EP is 1.6×10^{-1}, 7.2×10^{-2} and 9.3 $\times10^{-3}$ Pg C yr^{-1}, respectively. The estimation of global marine carbon uptake for new growth attributed to dust deposition is 5.6 Pg C yr^{-1}, which may be overestimated due to the assumption that every grid where dust deposition occurs over the ocean responds to its Fe supply. Therefore, the actual annual marine carbon uptake for new growth due to dust deposition worldwide is likely between 0.2 Pg C yr^{-1} and 5.6 Pg C yr^{-1}.

3.4 Source apportionments of carbon uptake for new growth induced by dust deposition

Dust from NEAf (1.7 Pg C yr^{-1}), NWAf (1.5 Pg C yr^{-1}), and WAs (1.3 Pg C yr^{-1}) are the primary drivers of marine carbon uptake for new growth induced by dust deposition (Fig. 12). NEAf, NWAf and WAs make their largest contributions to marine carbon uptake for new growth during the summer, contributing 0.7, 0.4 and 0.7 Pg C yr^{-1}, respectively (Fig. 12). They (NEAf, NWAf and WAs) all contribute least in autumn with contributions of 0.2, 0.2, and 0.1 Pg C yr^{-1}, respectively (Fig. 12). Examining the seasonal variation in contributions from dust sources to global dust-driven carbon uptake for new growth of marine phytoplankton, contribution from EAs exhibits the largest seasonal variation. In spring, marine carbon uptake for new growth induced by dust from EAs is about ten times higher than in winter (Fig. 12). Dust from MAf and MNAs also shows a 5-6 fold difference in their contributions to global marine carbon uptake for new growth across different seasons, but their overall contributions remain

https://doi.org/10.5194/egusphere-2025-763
Preprint. Discussion started: 6 March 2025

only ~2% (Fig. 12 and 13).

The heterogeneity in Fe solubility and Fe:C ratios across global oceans leads to difference in the contributions of dust sources to marine dust deposition and phytoplankton carbon uptake. The greatest contributors to carbon uptake for new growth in EP differ from those that contribute most to dust deposition in the region (Fig. 7 and 13). The dust from AU is the dominant contributor to carbon uptake for new growth driven by dust deposition over EP, accounting for 30.4%, while the dust from NWAf and NEAf, the major contributors to dust deposition over EP, only accounts for 17.2% and 15.6%, respectively (Fig. 7 and 13). Dust from AU is the third largest supplier of Fe to dust deposition over EP, following NWAf and NEAf. This is primarily because dust deposition over EP from NWAf and NEAf is mainly concentrated in the northeast, near the southwest coast of NAm, where Fe: C ratios are relatively higher compared to the areas dust from AU is deposited over EP (Fig. S9). The contribution (33.4%) of dust from AU to carbon uptake for new growth in SO is lower compared to its contribution (51.5%) to dust deposition over SO (compare Fig. 7 and Fig. 13), mainly due to high Fe: C ratio in the southeast of AU, which is the primary area of dust from AU deposit over SO (Fig. S9). On the contrary, the contributions of the dust from SAf to carbon uptake for new growth in SO is larger compared to its contributions to dust deposition owing to low Fe: C ratio in the southeast of SAf, where is the main regions of SAf's dust deposit over SO (Fig. S9). Therefore, spatial variations in Fe solubility and the Fe: C ratio will to some extent lead to differences between the spatial distribution characteristics of dust deposition and the resulting spatial distribution

https://doi.org/10.5194/egusphere-2025-763
Preprint. Discussion started: 6 March 2025

545 characteristics of marine carbon uptake for new growth. Globally, dust from NEAf is
546 the largest contributor to the marine carbon uptake driven by dust deposition which
547 accounts for 30.0% (1.7 Pg C yr^{-1}) (Fig. 10), followed by NWAf (1.5 Pg C yr^{-1}),
548 accounting for 26.2%. WAs (1.3 Pg C yr^{-1}) and SAs (0.4 Pg C yr^{-1}) are also important
549 sources to annual total marine carbon uptake for new growth induced by dust deposition,
550 accounting for 24.0% and 6.4%. Dust from AU and EAs account for 4.3% and 3.4% of
551 the global marine carbon uptake for new growth driven by dust deposition, dust from
552 SAf and MAf account for 3.4% and 3.2%, respectively. Dust from SAm, MNAs and
553 NAm contribute relatively lower to the marine carbon uptake for new growth driven by
554 dust deposition, less than 1%, respectively.

555 The seasonal variation in marine carbon uptake for new growth is most
556 pronounced in RS (Fig. 11). The highest carbon uptake for new growth in RS occurred
557 in summer at 0.3 Pg C, which is about ten times higher than in winter, resulting in a
558 drastic seasonal fluctuation occurred in RS (Fig. 11). During summer, dust deposition
559 over RS increases from almost all dust sources, particularly NEAf and WAs (Fig. S10).
560 Specifically, dust from NEAf contributes 0.2 Pg C, and dust from WAs contributes 0.1
561 Pg C to carbon uptake for new growth driven by dust deposition in RS. Additionally,
562 the lowest Fe: C ratio in RS further enhances the marine carbon uptake for new growth
563 driven by dust deposition during summer. During winter, dust deposition in RS
564 primarily from NEAf and WAs, could leading to 1.2×10^{-2} Pg C and 2.1×10^{-2} Pg C of
565 carbon uptake for new growth (Fig. S10). The carbon uptake for new growth induced
566 by dust deposition over NP and EI also exhibits large seasonal variations, with

https://doi.org/10.5194/egusphere-2025-763
Preprint. Discussion started: 6 March 2025

differences between seasons reaching 542.1% and 438.8%, respectively (Fig. 11). The highest carbon uptake for new growth driven by dust deposition in NP occurred in spring at 0.2 Pg C, while the lowest occurred in winter at 2.9×10^{-2} Pg C. The carbon uptake for new growth in NP throughout the year is predominantly attributed to the dust from Asia, particularly from EAs and SAs (Fig. S10). The pronounced seasonal variations in dust emissions from EAs and SAs are the primary reasons for the large seasonal changes in carbon uptake for new growth induced by dust deposition in the NP (Fig. 3). During summer, carbon uptake for new growth driven by dust deposition in EI peaks at 0.9 Pg C, contrasting with its lowest uptake in autumn at 0.2 Pg C (Fig. 11). This fluctuation is primarily driven by changes in dust deposition over EI (Fig. 6). Substantial dust from NEAf and WAs deposits in EI during summer, sharply diminishing in autumn (Fig. 8).

4 Discussion and conclusions

Identifying the contribution of dust sources to deposition over oceans is key to quantify the dust-borne input of dFe to the ocean, which is critical for understanding its impact on marine ecosystems, the carbon cycle, and climate. In this study, CESM was employed to identify the contributions of various dust source regions to dust deposition, revealing that EA and EI are the major contributors to global dust deposition over the ocean, with contributions of 41.6% and 23.7%, respectively. These contributions are primarily due to the westward transport of dust from NEAf and NWAf, the largest dust emission sources, to the EA region, and the dominant southward transport of dust from

https://doi.org/10.5194/egusphere-2025-763
Preprint. Discussion started: 6 March 2025

WAs to EI. Additionally, dust deposition over the RS exhibits the largest seasonal variations among ocean areas, with fluctuations of 626.3%, primarily due to a sudden large increase in deposited dust from NEAf over RS occurring exclusively in summer.

Based on the contribution relationship, we quantified the total Fe and dFe supplied to the ocean due to dust deposition and used the Fe: C ratio to identify its effect on carbon uptake for new growth by phytoplankton in various oceans, we found that dust deposition onto the ocean supplies 11.1 Tg yr^{-1} of Fe and 0.4 Tg yr^{-1} of dFe, leading to a marine carbon uptake for new growth of 5.6 Pg C yr^{-1}. Large marine carbon uptake for new growth driven by dust deposition occurs primarily in EA and EI, leading to 2.3 and 1.7 Pg C yr^{-1}, respectively, because large amount of dust deposition over EA and EI. Marine carbon uptake for new growth driven by dust deposition is highest in summer (2.1 Pg C $season^{-1}$), followed by spring (1.4 Pg C $season^{-1}$) and winter (1.2 Pg C $season^{-1}$), with the lowest uptake occurred in autumn (0.9 Pg C $season^{-1}$). Marine carbon uptake for new growth caused by dust deposition in summer over the RS is 843.0% higher than in other seasons, representing the largest seasonal variation among ocean areas. This significant variation is primarily due to the sharp increase in dust deposition from NEAf during summer and the lowest Fe: C ratio in RS. Compared with previous studies, Myriokefalitakis et al (2018) reported that total Fe emissions from dust sources in various models (CAM4, IMPACT, GEOS-Chem, and TM4-ECPL) ranged from 38 to 134 Tg total Fe yr^{-1}, with a mean value of 71.5 ± 43 Tg total Fe yr^{-1}, which is comparable with our result of 42.5 Tg Fe yr^{-1}. Their simulations of soluble Fe from mineral dust ranged from 0.3 to 1.0 Tg dFe yr^{-1}, with a mean value of

https://doi.org/10.5194/egusphere-2025-763
Preprint. Discussion started: 6 March 2025

approximately 0.7 ± 0.3 Tg dFe yr^{-1}. The amount of Fe supplied to the ocean from dust deposition in our study (11.1 Tg yr^{-1}) is close to the lower end of other global estimates (12.94 ± 0.31 Tg yr^{-1}) presented by Myriokefalitakis et al (2022).

Currently, few studies have quantified the large-scale response of the carbon cycle to dust deposition. Mahowald et al (2010) demonstrated that dust deposition trends increase ocean productivity by 6% over the 20th century, leading to marine carbon uptake of 8 Pg C (equivalent to 4ppm in atmospheric CO_2). Our result of marine carbon uptake for new growth induced by dust deposition is quite different grom the results indicated by Mahowald et al (2010), which is attributed to the different methodology employed. They combined the ecosystem component of the Biogeochemical Elemental Cycling (BEC) ocean model and a carbonate chemistry module to calculate pCO_2 and air-sea CO_2 flux to estimate the variation of carbon. However, their estimate of the influence on marine biogeochemistry was based on the increase of anthropogenic inorganic nitrogen and soluble Fe from atmospheric processing of dust and combustion sources, rather than from dust alone (Krishnamurthy et al., 2009). Our study refined the impact of dust deposition on marine carbon uptake and quantified the detailed contributions of different dust sources to different oceans in global scale. Moreover, Mahowald et al (2010) assumed a fixed Fe content in dust of 3.5% (Luo et al., 2008), while we applied different iron contents to various dust sources. If a fixed value of 3.5% were used, the estimated supply of dust-borne Fe to ocean would be increased by 76.6% compared to our current result (11.1 Tg yr^{-1}), based on our simulation of annual marine dust deposition (560.2 Tg yr^{-1}). Moreover, they considered only at hematite in dust as

https://doi.org/10.5194/egusphere-2025-763
Preprint. Discussion started: 6 March 2025

a source of dFe (Luo et al., 2008), which introduces considerable uncertainty compared to observations, potentially underestimating the impact of dust-borne Fe deposition on the carbon cycle. In this study, we interpolated and derived the spatial variability of Fe solubility based on extensive observational data. In comparison, the soluble Fe estimated by Mahowald et al (2010) took into account a combination of cloud processing, which could enhance the solubility of Fe due to acidity of cloud droplets (Luo et al., 2008). We used observed Fe solubility data over the ocean to estimate the dust-borne input of dFe, aiming to minimize the impact of complex atmospheric processes on Fe solubility. However, a gap remains between our estimates and the actual impact of atmospheric transport on Fe solubility. Future studies could quantify the impact of atmospheric transport on Fe solubility in Earth system model (Longo et al., 2016; Li et al., 2017; Luo et al., 2008). Moreover, ecological models, such as the BEC model, incorporate various potentially growth-limiting nutrients and have ability to simulate different phytoplankton functional groups, which could be compared to our evaluation. Westberry et al (2023) estimated that 2.55×10^{-2} Pg C yr^{-1} of primary production was supported by dust deposition onto the ocean, based on the Carbon-based Production Model (CbPM). The CbPM links net primary production to the product of phytoplankton carbon biomass and phytoplankton-specific growth rate, both of which are modeled based on the satellite-measured chlorophyll-to-carbon ratio and mixed-layer growth irradiance (Siegel et al., 2014). Satellite data is susceptible to the impacts of atmospheric conditions and cloud cover, and satellite ocean color products often rely on empirical models for inversion, which may lead to uncertainty compared to

https://doi.org/10.5194/egusphere-2025-763
Preprint. Discussion started: 6 March 2025

observations. Furthermore, they provided limited insights into the evaluation of dust-induced marine carbon uptake, lacking a detailed analysis of the spatiotemporal variations and sources of this carbon up on a global scale. Our evaluation of carbon uptake was based on simulated dust deposition combined with multiple observation datasets, including global distribution of marine Fe solubility, total Fe concentration in the oceans, which would provide diverse perspectives and comprehensive view of marine ecological response to dust emission over the world.

The uncertainty of annual marine carbon uptake for new growth due to dust deposition (5.6 ± 0.2 Pg C yr^{-1}) was estimated by interannual variations. The primary uncertainty is the interannual variability in the magnitude of marine dust deposition (approximately 550-600 Tg yr^{-1}) and its spatial distribution. Additionally, we also employed Coupled Model Intercomparison Project Phase (CMIP6) dFe concertation data to estimate the marine carbon uptake for new growth driven by dust deposition. The results indicated a marine carbon uptake of 2.2 Pg C yr^{-1} for new growth due to dust deposition (Fig. S11). Compared to the estimates of marine carbon uptake fore new growth due to dust deposition derived from observations, the distributions of marine carbon uptake associated to new growth because of dust deposition by CMIP6 and observations are similar on a global scale, with high values primarily occurring in the EA, exhibiting a characteristic decrease from east to west, and in the EI, particularly in the northwestern EI. The use of CMIP6 dFe concentration data resulted in a 60.7% reduction in marine carbon uptake for new growth driven by dust deposition, compared to estimates based on observations. This decrease was particularly pronounced in the

https://doi.org/10.5194/egusphere-2025-763
Preprint. Discussion started: 6 March 2025

southern RS, where uptake decreased from 0.4 to 0.1 Pg C yr^{-1}, the western Arabian Sea (in the EI), where it decreased from 1.8 to 0.5 Pg C yr^{-1}, and the north-central EA, where it decreased from 2.2 to 0.7 Pg C yr^{-1} (compare Fig. 9 and Fig. S11). Compared the result with that obtained using unfiltered Fe solubility data, the marine carbon uptake for new growth attributed to dust deposition decreased by 54.1%, as the largest range of Fe solubility shifted from 50.0% to 6.0%. Although uncertainty remains in estimating the marine carbon uptake for new growth attributed to dust deposition, it can still provide a meaningful reflection of potential requirements of phytoplankton, it does provide an observation-based quantification for the specific contributions of dust depositions to marine carbon uptakes.

In this study, we used data from 514 sites of Fe solubility and 3340 sites of dFe concentration across various oceans to interpolate and calculate the Fe: C ratio. However, the somewhat nonuniform distribution of marine observations across the vast spatial span of the study increases uncertainties in the interpolation of Fe solubility and dFe concentrations. Compared to dFe concentration, there is substantially less data available on the distribution of Fe solubility. More measurements and consistent measurement techniques would aid in the assessment of Fe solubility in the future. We assumed that phytoplankton in both HNLC and LNLC regions might respond to dust deposition as a maximum estimate, considering Fe is particularly important for nitrogen fixing phytoplankton in LNLC regions. However, the phytoplankton growth by dust addition in LNLC regions relies not only on Fe, but also on phosphorus. Therefore, future estimations in LNLC regions should account for other nutrients to achieve more

https://doi.org/10.5194/egusphere-2025-763
Preprint. Discussion started: 6 March 2025

accurate results. We assumed that every grid where dust deposition occurred over the ocean all responded to its Fe supply to estimate its impact on marine carbon uptake for new growth, but this response also depends on phytoplankton distribution and species, potentially leading to an overestimation of the marine ecological response to carbon uptake. Phytoplankton growth is not unlimited with an increase in Fe, which heightens the risk of overestimating the marine ecological response to carbon uptake in high dust regions. Therefore, a reasonable growth threshold should be considered based on further observations and experiments.

Data availability

GEOTRACES intermediate data is available athttps://www.bodc.ac.uk/geotraces/data/idp2021/.

Code availability

The codes used to produce these results are available from the corresponding author upon reasonable request.

Acknowledgments

This research has been supported by the National Key R&D Plan (Grant No.2022YFF0803000) and the National Natural Science Foundation of China (Grant No. 42177082).

Author contributions

JZ conceived the research; YL and JZ designed the experiments, performed model runs, and analyzed the data. YX, LC, QG and YS contributed to the preparation of the

https://doi.org/10.5194/egusphere-2025-763
Preprint. Discussion started: 6 March 2025

model input and data processing; PF and CL joined the discussion of the research; LC wrote the first draft of the manuscript; JZ and YL revised the manuscript before submission with contributions from all co-authors.

Competing Interests

The authors declare that they have no conflict of interest.

https://doi.org/10.5194/egusphere-2025-763
Preprint. Discussion started: 6 March 2025

References

Aumont, O. and Bopp, L.: Globalizing results from ocean in situ iron fertilization studies, Glob. Biogeochem. Cycles, 20, 10.1029/2005GB002591, 2006.

Bishop, J. K. B., Davis, R. E., and Sherman, J. T.: Robotic observations of dust storm enhancement of carbon biomass in the North Pacific, Science, 298, 817-821, 10.1126/science.1074961, 2002.

Boyd, P. W. and Ellwood, M. J.: The biogeochemical cycle of iron in the ocean, Nat. Geosci., 3, 675-682, 10.1038/ngeo964, 2010.

Boyd, P. W., Jickells, T., Law, C. S., Blain, S., Boyle, E. A., Buesseler, K. O., Coale, K. H., Cullen, J. J., de Baar, H. J. W., Follows, M., Harvey, M., Lancelot, C., Levasseur, M., Owens, N. P. J., Pollard, R., Rivkin, R. B., Sarmiento, J., Schoemann, V., Smetacek, V., Takeda, S., Tsuda, A., Turner, S., and Watson, A. J.: Mesoscale iron enrichment experiments 1993-2005: Synthesis and future directions, Science, 315, 612-617, 10.1126/science.1131669, 2007.

Choobari, O. A., Zawar-Reza, P., and Sturman, A.: The global distribution of mineral dust and its impacts on the climate system: A review, Atmos. Res., 138, 152-165, 10.1016/j.atmosres.2013.11.007, 2014.

Dietze, H., Getzlaff, J., and Loeptien, U.: Simulating natural carbon sequestration in the Southern Ocean: on uncertainties associated with eddy parameterizations and iron deposition, Biogeosciences, 14, 1561-1576, 10.5194/bg-14-1561-2017, 2017.

https://doi.org/10.5194/egusphere-2025-763
Preprint. Discussion started: 6 March 2025

749 Félix-Bermúdez, A., Delgadillo-Hinojosa, F., Torres-Delgado, E. V., and Munoz-
750 Barbosa, A.: Does Sea Surface Temperature Affect Solubility of Iron in M
751 ineral Dust? The Gulf of California as a Case Study, J. Geophys. Res. Oc
752 eans., 125, 10.1029/2019JC015999, 2020.
753 Gao, Y., Kaufman, Y. J., Tanré, D., Kolber, D., and Falkowski, P. G.: Seasona
754 l distributions of aeolian iron fluxes to the global ocean, Geophys. Res. L
755 ett., 28, 29-32, 10.1029/2000GL011926, 2001.
756 GEOTRACES Intermediate Data Product Group. The GEOTRACES intermediat
757 e data product 2021v2 (IDP2021v2). NERC EDS British Oceanographic D
758 ata Centre NOC. 10.5285/ff46f034-f47c-05f9-e053-6c86abc0dc7e (2023).
759 Ginoux, P., Chin, M., Tegen, I., Prospero, J. M., Holben, B., Dubovik, O., and
760 Lin, S. J.: Sources and distributions of dust aerosols simulated with the
761 GOCART model, J. Geophys. Res. Atmos., 106, 20255-20273, 10.1029/200
762 0JD000053, 2001.
763 Hamilton, D. S., Baker, A. R., Iwamoto, Y., Gasso, S., Bergas-Masso, E., Deut
764 ch, S., Dinasquet, J., Kondo, Y., Llort, J., Myriokefalitakis, S., Perron, M.
765 M. G., Wegmann, A., and Yoon, J.-E.: An aerosol odyssey: Navigating nu
766 trient flux changes to marine ecosystems, Elementa-Sci Anthrop., 11, 10.15
767 25/elementa.2023.00037, 2023.
768 Hamilton, D. S., Perron, M. M. G., Bond, T. C., Bowie, A. R., Buchholz, R.
769 R., Guieu, C., Ito, A., Maenhaut, W., Myriokefalitakis, S., Olgun, N., Rath
770 od, S. D., Schepanski, K., Tagliabue, A., Wagner, R., and Mahowald, N.

https://doi.org/10.5194/egusphere-2025-763
Preprint. Discussion started: 6 March 2025

M.: Earth, Wind, Fire, and Pollution: Aerosol Nutrient Sources and Impacts on Ocean Biogeochemistry, Annu. Rev. Mar. Sci., 14, 303-330, 10.1146/annurev-marine-031921-013612, 2022.

Hurrell, J. W., Holland, M. M., Gent, P. R., Ghan, S., Kay, J. E., Kushner, P. J., Lamarque, J. F., Large, W. G., Lawrence, D., Lindsay, K., Lipscomb, W. H., Long, M. C., Mahowald, N., Marsh, D. R., Neale, R. B., Rasch, P., Vavrus, S., Vertenstein, M., Bader, D., Collins, W. D., Hack, J. J., Kiehl, J., and Marshall, S.: The Community Earth System Model A Framework for Collaborative Research, Bull. Am. Meteorol. Soc., 94, 1339-1360, 10.1175/BAMS-D-12-00121.1, 2013.

Ito, A., Ye, Y., Yamamoto, A., Watanabe, M., and Aita, M. N.: Responses of ocean biogeochemistry to atmospheric supply of lithogenic and pyrogenic iron-containing aerosols, Geol. Mag., 157, 741-756, 10.1017/S0016756819001080, 2020.

Ito, A., Myriokefalitakis, S., Kanakidou, M., Mahowald, N. M., Scanza, R. A., Hamilton, D. S., Baker, A. R., Jickells, T., Sarin, M., Bikkina, S., Gao, Y., Shelley, R. U., Buck, C. S., Landing, W. M., Bowie, A. R., Perron, M. M. G., Guieu, C., Meskhidze, N., Johnson, M. S., Feng, Y., Kok, J. F., Nenes, A., and Duce, R. A.: Pyrogenic iron: The missing link to high iron solubility in aerosols, Sci. Adv., 5, 10.1126/sciadv.aau7671, 2019.

Jickells, T. D., An, Z. S., Andersen, K. K., Baker, A. R., Bergametti, G., Brooks, N., Cao, J. J., Boyd, P. W., Duce, R. A., Hunter, K. A., Kawahata,

https://doi.org/10.5194/egusphere-2025-763
Preprint. Discussion started: 6 March 2025

H., Kubilay, N., laRoche, J., Liss, P. S., Mahowald, N., Prospero, J. M., Ridgwell, A. J., Tegen, I., and Torres, R.: Global iron connections betwee n desert dust, ocean biogeochemistry, and climate, Science, 308, 67-71, 10. 1126/science.1105959, 2005.

Johnson, M. S. and Meskhidze, N.: Atmospheric dissolved iron deposition to th e global oceans: effects of oxalate-promoted Fe dissolution, photochemical redox cycling, and dust mineralogy, Geosci. Model Dev., 6, 1137-1155, 10. 5194/gmd-6-1137-2013, 2013.

Journet, E., Desboeufs, K. V., Caquineau, S., and Colin, J.-L.: Mineralogy as a critical factor of dust iron solubility, Geophys. Res. Lett. 35, 10.1029/200 7GL031589, 2008.

Kanakidou, M., Myriokefalitakis, S., and Tsigaridis, K.: Aerosols in atmospheri c chemistry and biogeochemical cycles of nutrients, Environ. Res. Lett. 13, 10.1088/1748-9326/aabcdb, 2018.

Kobayashi, H., Oka, A., Yamamoto, A., and Abe-Ouchi, A.: Glacial carbon cy cle changes by Southern Ocean processes with sedimentary amplification, Sci. Adv., 7, 10.1126/sciadv.abg7723, 2021.

Kok, J. F., Adebiyi, A. A., Albani, S., Balkanski, Y., Checa-Garcia, R., Chin, M., Colarco, P. R., Hamilton, D. S., Huang, Y., Ito, A., Klose, M., Leung, D. M., Li, L., Mahowald, N. M., Miller, R. L., Obiso, V., Perez Garcia-Pando, C., Rocha-Lima, A., Wan, J. S., and Whicker, C. A.: Improved rep resentation of the global dust cycle using observational constraints on dust

https://doi.org/10.5194/egusphere-2025-763
Preprint. Discussion started: 6 March 2025

properties and abundance, Atmos. Chem. Phys., 21, 8127-8167, 10.5194/acp-21-8127-2021, 2021.

Krishnamurthy, A., Moore, J. K., Mahowald, N., Luo, C., Doney, S. C., Lindsay, K., and Zender, C. S.: Impacts of increasing anthropogenic soluble iron and nitrogen deposition on ocean biogeochemistry, Global Biogeochem. Cycles, 23, 10.1029/2008GB003440, 2009.

Kurisu, M., Sakata, K., Nishioka, J., Obata, H., Conway, T. M., Hunt, H. R., Sieber, M., Suzuki, K., Kashiwabara, T., Kubo, S., Takada, M., and Takahashi, Y.: Source and fate of atmospheric iron supplied to the subarctic North Pacific traced by stable iron isotope ratios, Geochim. Cosmochim. Acta., 378, 168-185, 10.1016/j.gca.2024.06.009, 2024.

Lambert, F., Delmonte, B., Petit, J. R., Bigler, M., Kaufmann, P. R., Hutterli, M. A., Stocker, T. F., Ruth, U., Steffensen, J. P., and Maggi, V.: Dust-climate couplings over the past 800,000 years from the EPICA Dome C ice core, Nature, 452, 616-619, 10.1038/nature06763, 2008.

Li, W., Xu, L., Liu, X., Zhang, J., Lin, Y., Yao, X., Gao, H., Zhang, D., Chen, J., Wang, W., Harrison, R. M., Zhang, X., Shao, L., Fu, P., Nenes, A., and Shi, Z.: Air pollution-aerosol interactions produce more bioavailable iron for ocean ecosystems, Sci. Adv., 3, 10.1126/sciadv.1601749, 2017.

Longo, A. F., Feng, Y., Lai, B., Landing, W. M., Shelley, R. U., Nenes, A., Mihalopoulos, N., Violaki, K., and Ingall, E. D.: Influence of Atmospheric Processes on the Solubility and Composition of Iron in Saharan Dust, En

https://doi.org/10.5194/egusphere-2025-763
Preprint. Discussion started: 6 March 2025

viron. Sci. Technol., 50, 6912-6920, 10.1021/acs.est.6b02605, 2016.

Luo, C., Mahowald, N., Bond, T., Chuang, P. Y., Artaxo, P., Siefert, R., Chen, Y., and Schauer, J.: Combustion iron distribution and deposition, Global Biogeochem. Cycles, 22, 10.1029/2007GB002964, 2008.

Mahowald, N.: Aerosol Indirect Effect on Biogeochemical Cycles and Climate, Science, 334, 794-796, 10.1126/science.1207374, 2011.

Mahowald, N. M., Muhs, D. R., Levis, S., Rasch, P. J., Yoshioka, M., Zender, C. S., and Luo, C.: Change in atmospheric mineral aerosols in response to climate: Last glacial period, preindustrial, modern, and doubled carbon di oxide climates, J. Geophys. Res. Atmos., 111, 10.1029/2005JD006653, 200 6.

Mahowald, N. M., Scanza, R., Brahney, J., Goodale, C. L., Hess, P. G., Moor e, J. K., and Neff, J.: Aerosol Deposition Impacts on Land and Ocean Ca rbon Cycles, Curr. Clim. Change Rep., 3, 16-31, 10.1007/s40641-017-0056- z, 2017.

Mahowald, N. M., Baker, A. R., Bergametti, G., Brooks, N., Duce, R. A., Jick ells, T. D., Kubilay, N., Prospero, J. M., and Tegen, I.: Atmospheric globa l dust cycle and iron inputs to the ocean, Global Biogeochem. Cycles, 19, 10.1029/2004GB002402, 2005.

Mahowald, N. M., Engelstaedter, S., Luo, C., Sealy, A., Artaxo, P., Benitez-Nel son, C., Bonnet, S., Chen, Y., Chuang, P. Y., Cohen, D. D., Dulac, F., He rut, B., Johansen, A. M., Kubilay, N., Losno, R., Maenhaut, W., Paytan,

https://doi.org/10.5194/egusphere-2025-763
Preprint. Discussion started: 6 March 2025

A., Prospero, J. A., Shank, L. M., and Siefert, R. L.: Atmospheric Iron D
eposition: Global Distribution, Variability, and Human Perturbations, Annu.
Rev. Mar. Sci., 1, 245-278, 10.1146/annurev.marine.010908.163727, 2009.

Mahowald, N. M., Kloster, S., Engelstaedter, S., Moore, J. K., Mukhopadhyay,
S., McConnell, J. R., Albani, S., Doney, S. C., Bhattacharya, A., Curran,
M. A. J., Flanner, M. G., Hoffman, F. M., Lawrence, D. M., Lindsay, K.,
Mayewski, P. A., Neff, J., Rothenberg, D., Thomas, E., Thornton, P. E., a
nd Zender, C. S.: Observed 20th century desert dust variability: impact on
climate and biogeochemistry, Atmos. Chem. Phys., 10, 10875-10893, 10.51
94/acp-10-10875-2010, 2010.

Mahowald, N. M. & Luo, C. A less dusty future? Geophys. Res. Lett. 30, 190
3, 10.1029/2003GL017880, 2003.

Matrin, J. H. Glacial-interglacial CO_2 change: the iron hypothesis. Paleoceanogr
aphy, 5, 1-13, 10.1029/PA005i001p00001, 1990.

Mills, M. M., Ridame, C., Davey, M., La Roche, J., and Geider, R. J.: Iron a
nd phosphorus co-limit nitrogen fixation in the eastern tropical North Atla
ntic, Nature, 429, 292-294, 10.1038/nature02550, 2004.

Moore, C. M., Mills, M. M., Arrigo, K. R., Berman-Frank, I., Bopp, L., Boyd,
P. W., Galbraith, E. D., Geider, R. J., Guieu, C., Jaccard, S. L., Jickells,
T. D., La Roche, J., Lenton, T. M., Mahowald, N. M., Maranon, E., Mar
inov, I., Moore, J. K., Nakatsuka, T., Oschlies, A., Saito, M. A., Thingsta
d, T. F., Tsuda, A., and Ulloa, O.: Processes and patterns of oceanic nutri

https://doi.org/10.5194/egusphere-2025-763
Preprint. Discussion started: 6 March 2025

881 ent limitation, Nat. Geosci., 6, 701-710, 10.1038/NGEO1765, 2013.
882 Myriokefalitakis, S., Daskalakis, N., Mihalopoulos, N., Baker, A. R., Nenes, A.,
883 and Kanakidou, M.: Changes in dissolved iron deposition to the oceans d
884 riven by human activity: a 3-D global modelling study, Biogeosciences, 12,
885 3973-3992, 10.5194/bg-12-3973-2015, 2015.
886 Myriokefalitakis, S., Bergas-Masso, E., Goncalves-Ageitos, M., Garcia-Pando, C.
887 P., van Noije, T., Le Sager, P., Ito, A., Athanasopoulou, E., Nenes, A., K
888 anakidou, M., Krol, M. C., and Gerasopoulos, E.: Multiphase processes in
889 the EC-Earth model and their relevance to the atmospheric oxalate, sulfate,
890 and iron cycles, Geosci. Model Dev., 15, 3079-3120, 10.5194/gmd-15-307
891 9-2022, 2022.
892 Myriokefalitakis, S., Ito, A., Kanakidou, M., Nenes, A., Krol, M. C., Mahowal
893 d, N. M., Scanza, R. A., Hamilton, D. S., Johnson, M. S., Meskhidze, N.,
894 Kok, J. F., Guieu, C., Baker, A. R., Jickells, T. D., Sarin, M. M., Bikkin
895 a, S., Shelley, R., Bowie, A., Perron, M. M. G., and Duce, R. A.: Revie
896 ws and syntheses: the GESAMP atmospheric iron deposition model interco
897 mparison study, Biogeoscience, 15, 6659-6684, 10.5194/bg-15-6659-2018, 2
898 018.
899 Okin, G. S., Baker, A. R., Tegen, I., Mahowald, N. M., Dentener, F. J., Duce,
900 R. A., Galloway, J. N., Hunter, K., Kanakidou, M., Kubilay, N., Prospero,
901 J. M., Sarin, M., Surapipith, V., Uematsu, M., and Zhu, T.: Impacts of at
902 mospheric nutrient deposition on marine productivity: Roles of nitrogen, ph

https://doi.org/10.5194/egusphere-2025-763
Preprint. Discussion started: 6 March 2025

osphorus, and iron, Glob. Biogeochem. Cycles, 25, 10.1029/2010GB003858, 2011.

Oleson, W., Lawrence, M., Bonan, B., Flanner, G., Kluzek, E., Lawrence, J., L evis, S., Swenson, C., Thornton, E., Dai, A., Decker, M., Dickinson, R., F eddema, J., Heald, L., Hoffman, F., Lamarque, J., Mahowald, N., Niu, G., Qian, T. T., Randerson, J., Running, S., Sakaguchi, K., Slater, A., Stöckli, R., Wang, A. H., Yang, Z. L., Zeng, X., Zeng, X.. Technical Description of version 4.0 of the Community Land Model (CLM) (No. NCAR/TN-478 +STR). University Corporation for Atmospheric Research, 10.5065/D6FB50 WZ, 2010.

Patra, P. K., Moore, J. K., Mahowald, N., Uematsu, M., Doney, S. C., and Na kazawa, T.: Exploring the sensitivity of interannual basin-scale air-sea CO_2 fluxes to variability in atmospheric dust deposition using ocean carbon cyc le models and atmospheric CO_2 inversions, J. Geophys. Res. Biogeoscience s, 112, 10.1029/2006JG000236, 2007.

Pavia, F. J., Anderson, R. F., Winckler, G., and Fleisher, M. Q.: Atmospheric Dust Inputs, Iron Cycling, and Biogeochemical Connections in the South P acific Ocean from Thorium Isotopes, Glob. Biogeochem. Cycles, 34, 10.10 29/2020GB006562, 2020.

Poulton, S. W. and Raiswell, R.: The low-temperature geochemical cycle of iro n: From continental fluxes to marine sediment deposition, Am. J. Sci., 30 2, 774-805, 10.2475/ajs.302.9.774, 2002.

https://doi.org/10.5194/egusphere-2025-763
Preprint. Discussion started: 6 March 2025

925 Raiswell, R. and Canfield, D. E.: The iron biogeochemical cycle past and pres
926 ent, Geochem. Perspect., 1, 1-220, 10.7185/geochempersp.1.1, 2012.
927 Scanza, R. A., Hamilton, D. S., Perez Garcia-Pando, C., Buck, C., Baker, A.,
928 and Mahowald, N. M.: Atmospheric processing of iron in mineral and co
929 mbustion aerosols: development of an intermediate-complexity mechanism s
930 uitable for Earth system models, Atmos. Chem. Phys., 18, 14175-14196, 1
931 0.5194/acp-18-14175-2018, 2018.
932 Schlitzer, R., Anderson, R. F., Dodas, E. M., Lohan, M., Geibere, W., Tagliabu
933 e, A., Bowie, A., Jeandel, C., Maldonado, M. T., Landing, W. M., Cockw
934 ell, D., Abadie, C., Abouchami, W., Achterberg, E. P., Agather, A., Agulia
935 r-Islas, A., van Aken, H. M., Andersen, M., Archer, C., Auro, M., de Baa
936 r, H. J., Baars, O., Baker, A. R., Bakker, K., Basak, C., Baskaran, M., Ba
937 tes, N. R., Bauch, D., van Beek, P., Behrens, M. K., Black, E., Bluhm,
938 K., Bopp, L., Bouman, H., Bowman, K., Bown, J., Boyd, P., Boye, M., B
939 oyle, E. A., Branellec, P., Bridgestock, L., Brissebrat, G., Browning, T., B
940 ruland, K. W., Brumsack, H.-J., Brzezinski, M., Buck, C. S., Buck, K. N.,
941 Buesseler, K., Bull, A., Butler, E., Cai, P., Camara Mor, P., Cardinal, D.,
942 Carlson, C., Carrasco, G., Casacuberta, N., Casciotti, K. L., Castrillejo, M.,
943 Chamizo, E., Chance, R., Charette, M. A., Chaves, J. E., Cheng, H., Che
944 ver, F., Christl, M., Church, T. M., Closset, I., Colman, A., Conway, T.
945 M., Cossa, D., Croot, P., Cullen, J. T., Cutter, G. A., Daniels, C., Dehairs,
946 F., Deng, F., Dieu, H. T., Duggan, B., Dulaquais, G., Dumousseaud, C.,

https://doi.org/10.5194/egusphere-2025-763
Preprint. Discussion started: 6 March 2025

947 Echegoyen-Sanz, Y., Edwards, R. L., Ellwood, M., Fahrbach, E., Fitzsimm
948 ons, J. N., Flegal, A. R., Fleisher, M. Q., van de Flierdt, T., Frank, M., F
949 riedrich, J., Fripiat, F., Froellje, H., Galer, S. J. G., Gamo, T., Ganeshram,
950 R. S., Garcia-Orellana, J., Garcia-Solsona, E., Gault-Ringold, M., George,
951 E., Gerringa, L. J. A., Gilbert, M., Godoy, J. M., Goldstein, S. L., Gonzal
952 ez, S. R., Grissom, K., Hammerschmidt, C., Hartman, A., Hassler, C. S.,
953 Hathorne, E. C., Hatta, M., Hawco, N., Hayes, C. T., Heimburger, L.-E.,
954 Helgoe, J., Heller, M., Henderson, G. M., Henderson, P. B., van Heuven,
955 S., Ho, P., Horner, T. J., Hsieh, Y.-T., Huang, K.-F., Humphreys, M. P., Is
956 shiki, K., Jacquot, J. E., Janssen, D. J., Jenkins, W. J., John, S., Jones, E.
957 M., Jones, J. L., Kadko, D. C., Kayser, R., Kenna, T. C., Khondoker, R.,
958 Kim, T., Kipp, L., Klar, J. K., Klunder, M., Kretschmer, S., Kumamoto,
959 Y., Laan, P., Labatut, M., Lacan, F., Lam, P. J., Lambelet, M., Lamborg,
960 C. H., Le Moigne, F. A. C., Le Roy, E., Lechtenfeld, O. J., Lee, J.-M., L
961 herminier, P., Little, S., Lopez-Lora, M., Lu, Y., Masque, P., Mawji, E., M
962 cClain, C. R., Measures, C., Mehic, S., Menzel Barraqueta, J.-L., van der
963 Merwe, P., Middag, R., Mieruch, S., Milne, A., Minami, T., Moffett, J.
964 W., Moncoiffe, G., Moore, W. S., Morris, P. J., Morton, P. L., Nakaguchi,
965 Y., Nakayama, N., Niedermiller, J., Nishioka, J., Nishiuchi, A., Noble, A.,
966 Obata, H., Ober, S., Ohnemus, D. C., van Ooijen, J., O'Sullivan, J., Owe
967 ns, S., Pahnke, K., Paul, M., Pavia, F., Pena, L. D., Petersh, B., Planchon,
968 F., Planquette, H., Pradoux, C., Puigcorbe, V., Quay, P., Queroue, F., Rad

https://doi.org/10.5194/egusphere-2025-763
Preprint. Discussion started: 6 March 2025

ic, A., Rauschenberg, S., Rehkamper, M., Rember, R., Remenyi, T., Resing, J. A., Rickli, J., Rigaud, S., Rijkenberg, M. J. A., Rintoul, S., Robinson, L. F., Roca-Marti, M., Rodellas, V., Roeske, T., Rolison, J. M., Rosenberg, M., Roshan, S., van der Loaff, M. M. R., Ryabenko, E., Saito, M. A., Salt, L. A., Sanial, V., Sarthou, G., Schallenberg, C., Schauer, U., Scher, H., Schlosser, C., Schnetger, B., Scott, P., Sedwick, P. N., Semiletov, I., Shelley, R., Sherrell, R. M., Shiller, A. M., Sigman, D. M., Singh, S. K., Slagter, H. A., Slater, E., Smethie, W. M., Snaith, H., Sohrin, Y., Sohst, B., Sonke, J. E., Speich, S., Steinfeldt, R., Stewart, G., Stichel, T., Stirling, C. H., Stutsman, J., Swarr, G. J., Swift, J. H., Thomas, A., Thorne, K., Till, C. P., Till, R., Townsend, A. T., Townsend, E., Tuerena, R., Twining, B. S., Vance, D., Velazquez, S., Venchiarutti, C., Villa-Alfageme, M., Vivancos, S. M., Voelker, A. H. L., Wake, B., Warner, M. J., Watson, R., van Weerlee, E., Weigand, M. A., Weinstein, Y., Weiss, D., Wisotzki, A., Woodward, E. M. S., Wu, J., Wu, Y., Wuttig, K., Wyatt, N., Xiang, Y., Xie, R. C., Xue, Z., Yoshikawa, H., Zhang, J., Zhang, P., Zhao, Y., Zheng, L., Zheng, X.-Y., Zieringer, M., Zimmer, L. A., Ziveri, P., Zunino, P., and Zurbrick, C.: The GEOTRACES Intermediate Data Product 2017, CHEMICAL GEOLOGY, 493, 210-223, 10.1016/j.chemgeo.2018.05.040, 2018.

Shaked, Y., Kustka, A. B., and Morel, F. M. M.: A general kinetic model for iron acquisition by eukaryotic phytoplankton, Limnol. Oceanogr., 50, 872-882, 10.4319/lo.2005.50.3.0872, 2005.

https://doi.org/10.5194/egusphere-2025-763
Preprint. Discussion started: 6 March 2025

991 Shi, Z., Krom, M. D., Bonneville, S., Baker, A. R., Jickells, T. D., and Benni
992 ng, L. G.: Formation of Iron Nanoparticles and Increase in Iron Reactivity
993 in Mineral Dust during Simulated Cloud Processing, Environ. Sci. Techno
994 l, 43, 6592-6596, 10.1021/es901294g, 2009.
995 Shi, Z., Krom, M. D., Jickells, T. D., Bonneville, S., Carslaw, K. S., Mihalopo
996 ulos, N., Baker, A. R., and Benning, L. G.: Impacts on iron solubility in
997 the mineral dust by processes in the source region and the atmosphere: A
998 review, Aeolian Res., 5, 21-42, 10.1016/j.aeolia.2012.03.001, 2012.
999 Shi, Z. B., Woodhouse, M. T., Carslaw, K. S., Krom, M. D., Mann, G. W., B
1000 aker, A. R., Savov, I., Fones, G. R., Brooks, B., Drake, N., Jickells, T.
1001 D., and Benning, L. G.: Minor effect of physical size sorting on iron solu
1002 bility of transported mineral dust, Atmos. Chem. Phys., 11, 8459-8469, 10.
1003 5194/acp-11-8459-2011, 2011a.
1004 Shi, Z., Krom, M. D., Bonneville, S., Baker, A. R., Bristow, C., Drake, N., M
1005 ann, G., Carslaw, K., McQuaid, J. B., Jickells, T., and Benning, L. G.: Inf
1006 luence of chemical weathering and aging of iron oxides on the potential ir
1007 on solubility of Saharan dust during simulated atmospheric processing, Glo
1008 bal Biogeochem. Cycles, 25, 10.1029/2010GB003837, 2011b.
1009 Shoenfelt, E. M., Winckler, G., Annett, A. L., Hendry, K. R., and Bostick, B.
1010 C.: Physical Weathering Intensity Controls Bioavailable Primary Iron (II) S
1011 ilicate Content in Major Global Dust Sources, Geophys. Res. Lett., 46, 10
1012 854-10864, 10.1029/2019GL084180, 2019.

https://doi.org/10.5194/egusphere-2025-763
Preprint. Discussion started: 6 March 2025

Siegel, D. A., Buesseler, K. O., Doney, S. C., Sailley, S. F., Behrenfeld, M. J., and Boyd, P. W.: Global assessment of ocean carbon export by combining satellite observations and food-web models, Global Biogeochem. Cycles, 28, 181-196, 10.1002/2013GB004743, 2014.

Spolaor, A., Vallelonga, P., Cozzi, G., Gabrieli, J., Varin, C., Kehrwald, N., Zennaro, P., Boutron, C., and Barbante, C.: Iron speciation in aerosol dust influences iron bioavailability over glacial-interglacial timescales, Geophys. Res. Lett., 40, 1618-1623, 10.1002/grl.50296, 2013.

Struve, T., Longman, J., Zander, M., Lamy, F., Winckler, G., and Pahnke, K.: Systematic changes in circumpolar dust transport to the Subantarctic Pacific Ocean over the last two glacial cycles, Proc. Natl. Acad. Sci. U.S.A., 119, 10.1073/pnas.2206085119, 2022.

Tagliabue, A., Bowie, A. R., Boyd, P. W., Buck, K. N., Johnson, K. S., and Saito, M. A.: The integral role of iron in ocean biogeochemistry, Nature, 543, 51-59, 10.1038/nature21058, 2017.

Tagliabue, A., Aumont, O., DeAth, R., Dunne, J. P., Dutkiewicz, S., Galbraith, E., Misumi, K., Moore, J. K., Ridgwell, A., Sherman, E., Stock, C., Vichi, M., Voelker, C., and Yool, A.: How well do global ocean biogeochemistry models simulate dissolved iron distributions? Global Biogeochem. Cycles, 30, 149-174, 10.1002/2015GB005289, 2016.

Tegen, I., Werner, M., Harrison, S. P., and Kohfeld, K. E.: Relative importance of climate and land use in determining present and future global soil dus

https://doi.org/10.5194/egusphere-2025-763
Preprint. Discussion started: 6 March 2025

t emission, Geophys. Res. Lett., 31, 10.1029/2003GL019216, 2004.

Trapp, J. M., Millero, F. J., and Prospero, J. M.: Trends in the solubility of ir on in dust-dominated aerosols in the equatorial Atlantic trade winds: Impo rtance of iron speciation and sources, Geochem. Geophys. Geosystems, 11, 10.1029/2009GC002651, 2010.

Twining, B. S., Rauschenberg, S., Morton, P. L., and Vogt, S.: Metal contents of phytoplankton and labile particulate material in the North Atlantic Ocea n, Prog. Oceanogr., 137, 261-283, 10.1016/j.pocean.2015.07.001, 2015.

Wang, N. and Zhang, Y.: Long-term variations of global dust emissions and cli mate control, Environ. Pollut., 340, 10.1016/j.envpol.2023.122847, 2024.

Watson, A. J., Bakker, D. C. E., Ridgwell, A. J., Boyd, P. W., and Law, C. S.: Effect of iron supply on Southern Ocean CO_2 uptake and implications fo r glacial atmospheric CO_2, Nature, 407, 730-733, 10.1038/35037561, 2000.

Westberry, T. K., Behrenfeld, M. J., Shi, Y. R., Yu, H., Remer, L. A., and Bia n, H.: Atmospheric nourishment of global ocean ecosystems, Science, 380, 515-519, 10.1126/science.abq5252, 2023.

Wiseman, N. A., Moore, J. K., Twining, B. S., Hamilton, D. S., and Mahowal d, N. M.: Acclimation of phytoplankton Fe:C ratios dampens the biogeoch emical response to varying atmospheric deposition of soluble iron, Global Biogeochem. Cycles, 37, 10.1029/2022GB007491, 2023.

Wolff, E. W., Barbante, C., Becagli, S., Bigler, M., Boutron, C. F., Castellano, E., de Angelis, M., Federer, U., Fischer, H., Fundel, F., Hansson, M., Hutt

https://doi.org/10.5194/egusphere-2025-763
Preprint. Discussion started: 6 March 2025

erli, M., Jonsell, U., Karlin, T., Kaufmann, P., Lambert, F., Littot, G. C., Mulvaney, R., Roethlisberger, R., Ruth, U., Severi, M., Siggaard-Andersen, M. L., Sime, L. C., Steffensen, J. P., Stocker, T. F., Traversi, R., Twarloh, B., Udisti, R., Wagenbach, D., and Wegner, A.: Changes in environment over the last 800,000 years from chemical analysis of the EPICA Dome C ice core, Quat. Sci. Rev., 29, 285-295, 10.1016/j.quascirev.2009.06.013, 2010.

Zender, C. S., Bian, H. S., and Newman, D.: Mineral Dust Entrainment and Deposition (DEAD) model: Description and 1990s dust climatology, J. Geophys. Res. Atmos., 108, 10.1029/2002JD002775, 2003.

Zhang, C., Yao, X., Chen, Y., Chu, Q., Yu, Y., Shi, J., and Gao, H.: Variations in the phytoplankton community due to dust additions in eutrophication, LNLC and HNLC oceanic zones, Sci. Total Environ., 669, 282-293, 10.1016/j.scitotenv.2019.02.068, 2019.

Zhang, Y., Mahowald, N., Scanza, R. A., Journet, E., Desboeufs, K., Albani, S., Kok, J. F., Zhuang, G., Chen, Y., Cohen, D. D., Paytan, A., Patey, M. D., Achterberg, E. P., Engelbrecht, J. P., and Fomba, K. W.: Modeling the global emission, transport and deposition of trace elements associated with mineral dust, Biogeosciences, 12, 5771-5792, 10.5194/bg-12-5771-2015, 2015.

Zheng, Y., Zhao, T., Che, H., Liu, Y., Han, Y., Liu, C., Xiong, J., Liu, J., and Zhou, Y.: A 20-year simulated climatology of global dust aerosol depositi

https://doi.org/10.5194/egusphere-2025-763
Preprint. Discussion started: 6 March 2025

on, Sci. Total Environ., 557, 861-868, 10.1016/j.scitotenv.2016.03.086, 2016.

Ziegler, M., Diz, P., Hall, I. R., and Zahn, R.: Millennial-scale changes in atmospheric CO_2 levels linked to the Southern Ocean carbon isotope gradient and dust flux, Nat. Geosci., 6, 457-461, 10.1038/NGEO1782, 2013.

https://doi.org/10.5194/egusphere-2025-763
Preprint. Discussion started: 6 March 2025

Figures

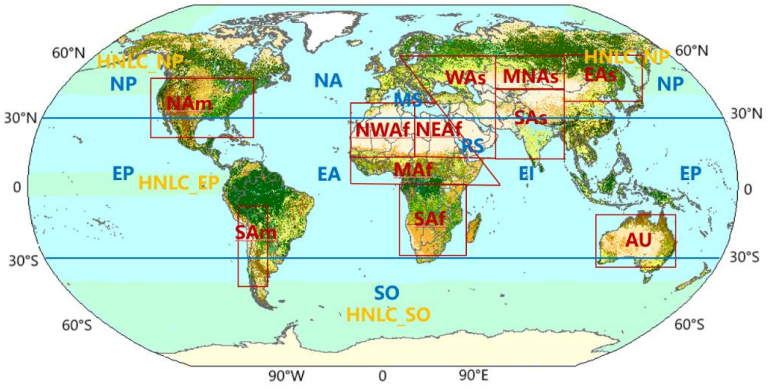

Fig. 1 The classification of global main dust source regions and oceans
(Dust source regions: NWAf - Northwest Africa; NEAf - Northeast Africa; MAf - Middle Africa; SAf - South Africa; NAm - North America; SAm - South America; WAs - West Asia; MNAs - Middle-North Asia; EAs - East Asia; SAs - South Asia; AU - Australia.)
(Oceans: NP - North Pacific Ocean; NA - North Atlantic Ocean; MS - Mediterranean Sea; SO - Southern Ocean; EP - Equatorial Pacific Ocean; EA - Equatorial Atlantic Ocean; EI - Equatorial Indian Ocean; HNLC_EP - high nutrient, low chlorophyll regions in Equatorial Pacific Ocean; HNLC_NP - high nutrient, low chlorophyll regions in North Pacific Ocean.)

https://doi.org/10.5194/egusphere-2025-763
Preprint. Discussion started: 6 March 2025

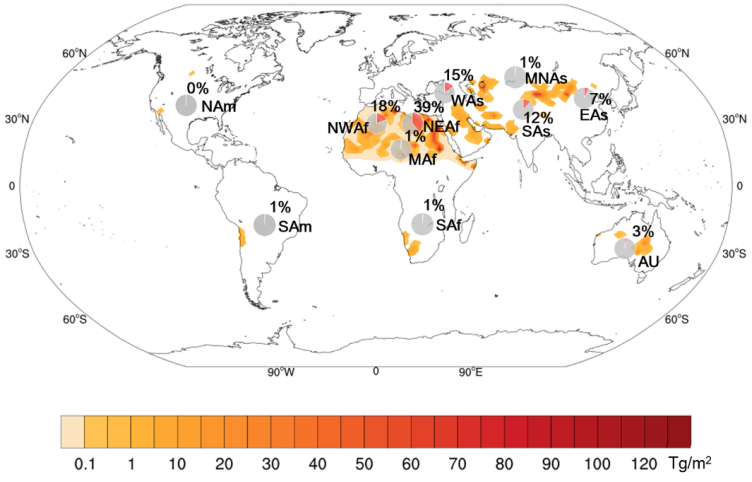

Fig. 2 The spatial distribution and proportion of the global five-year average dust emission, and pie charts show the proportions of annual dust emission of each dust source to global (Dust source regions: NWAf - Northwest Africa; NEAf - Northeast Africa; MAf - Middle Africa; SAf - South Africa; NAm - North America; SAm - South America; WAs - West Asia; MNAs - Middle-North Asia; EAs - East Asia; SAs - South Asia; AU - Australia.)

1091
1092

https://doi.org/10.5194/egusphere-2025-763
Preprint. Discussion started: 6 March 2025

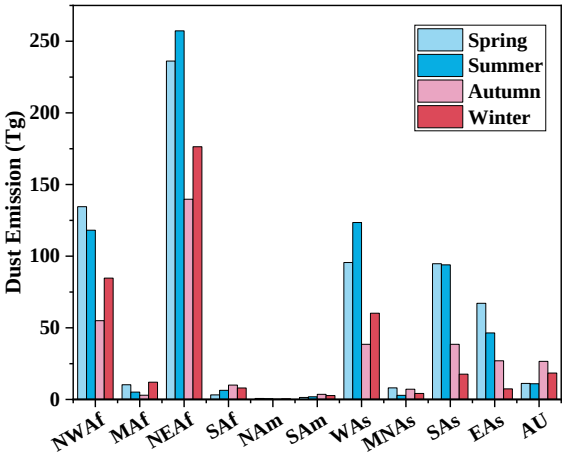

Fig. 3 The seasonal variations of dust emission in various dust sources

1093

1094

https://doi.org/10.5194/egusphere-2025-763
Preprint. Discussion started: 6 March 2025

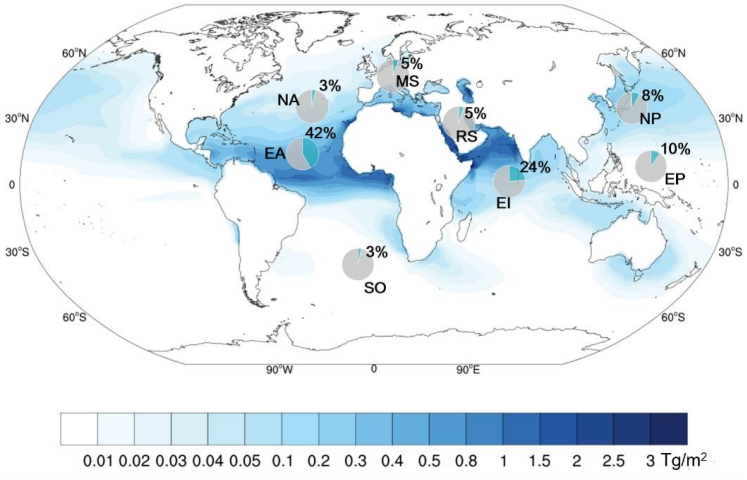

Fig. 4 The spatial distribution and proportion of the global five-year average dust deposition. Pie charts express the proportions of annual dust deposition in each ocean to global ocean
(Oceans: NP - North Pacific Ocean; NA - North Atlantic Ocean; MS - Mediterranean Sea; SO - Southern Ocean; EP - Equatorial Pacific Ocean; EA - Equatorial Atlantic Ocean; EI - Equatorial Indian Ocean.)

1095

1096

https://doi.org/10.5194/egusphere-2025-763
Preprint. Discussion started: 6 March 2025

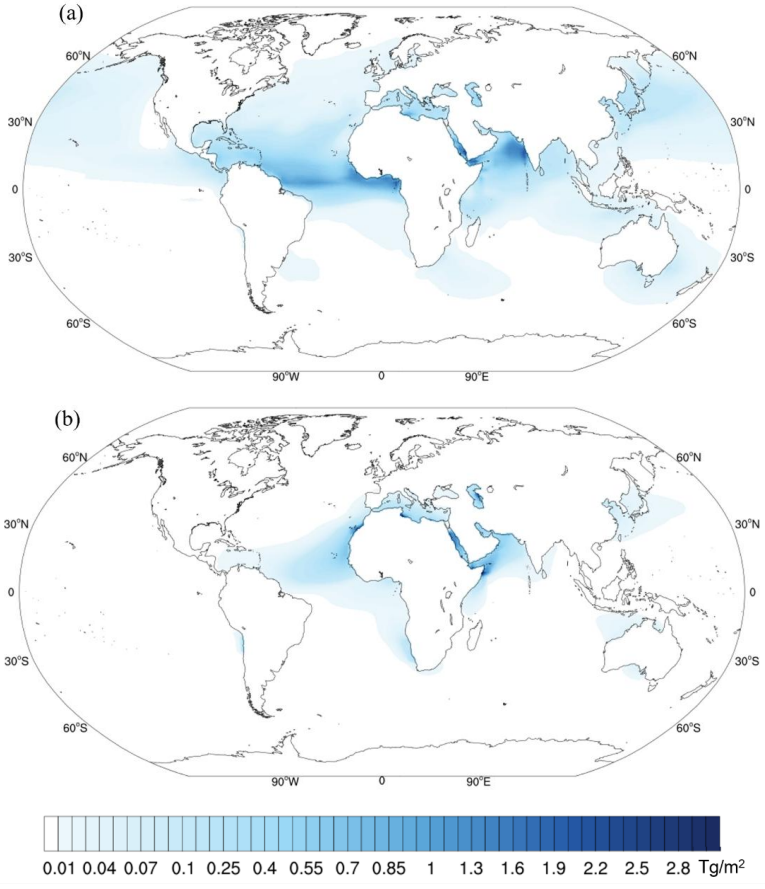

Fig. 5 The spatial distribution of the global five-year average dust (a) wet d eposition, and (b) dry deposition

1097

https://doi.org/10.5194/egusphere-2025-763
Preprint. Discussion started: 6 March 2025

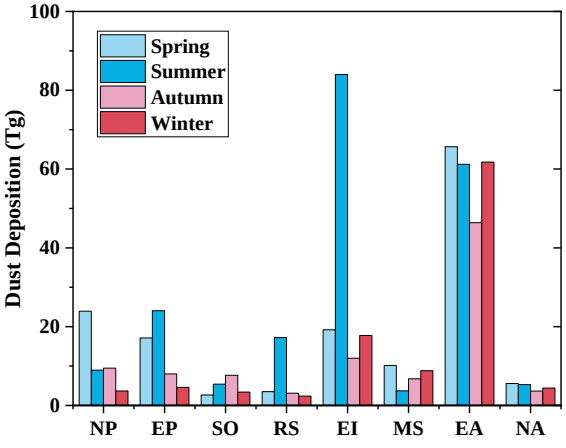

Fig. 6 The seasonal variations of dust deposition in various oceans

1098

1099

https://doi.org/10.5194/egusphere-2025-763
Preprint. Discussion started: 6 March 2025

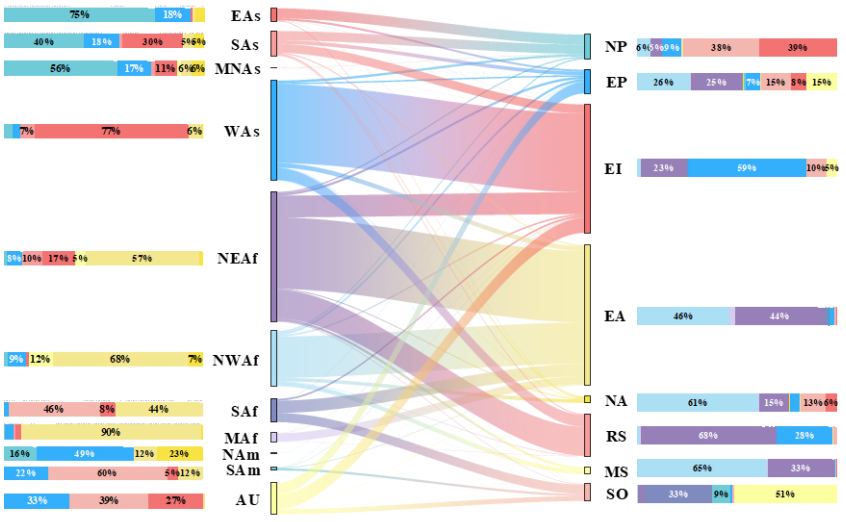

Fig. 7 The annual contributions of various dust source regions to oceanic dust deposition

The left lateral columns are the proportions of dust emitted from each dust source that deposits over each ocean, with different colors representing different oceans. The right lateral columns indicate the contributions from various dust sources to dust deposition over each ocean, different color corresponding to different dust sources. The longitudinal columns depict the proportions of dust emission or deposition relative to global marine dust deposition. The lines in the middle illustrate the transport direction and intensity.

1100

https://doi.org/10.5194/egusphere-2025-763
Preprint. Discussion started: 6 March 2025

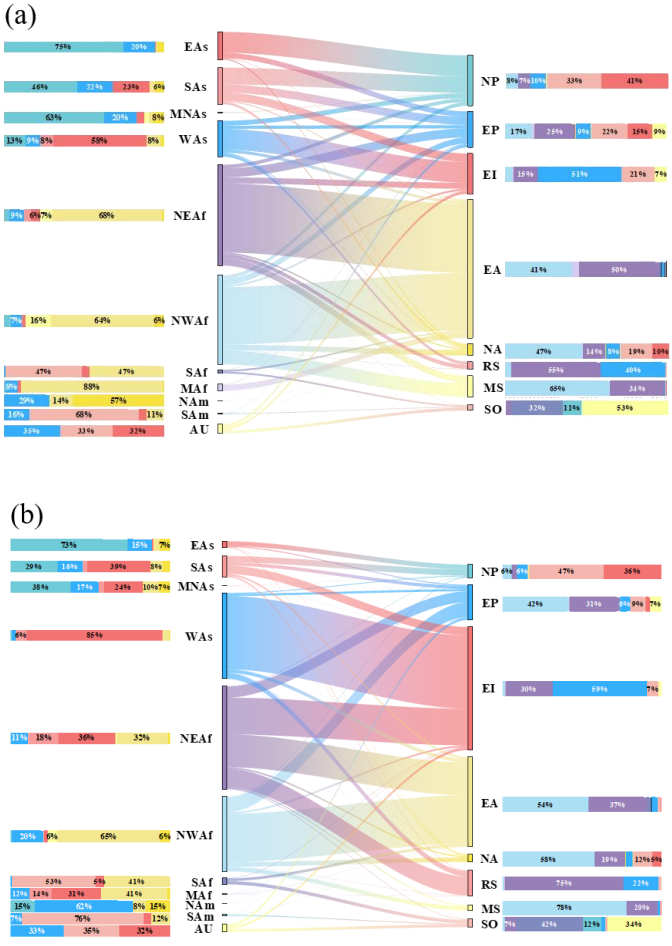

https://doi.org/10.5194/egusphere-2025-763
Preprint. Discussion started: 6 March 2025

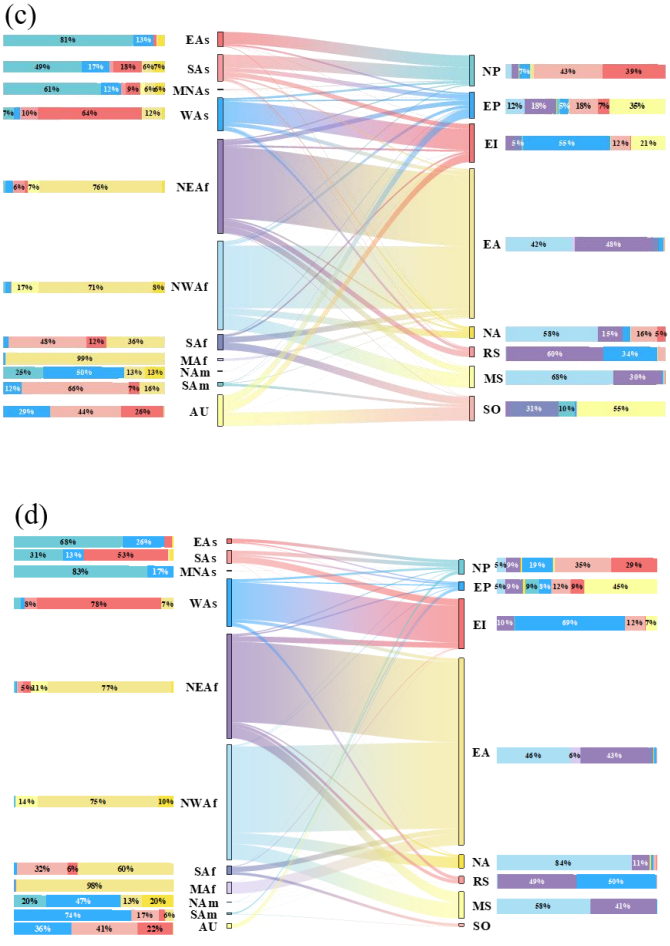

Fig. 8 The seasonal contributions of various dust source regions to oceanic dust deposition.
(a) spring; (b) summer; (c) autumn; (d) winter.
The left lateral columns are the proportions of dust emitted from each dust source that deposits over each ocean, with different colors representing different oceans. The right lateral columns indicate the contributions from various dust sources to dust deposition over each ocean, different color corresponding to different dust sources. The longitudinal columns depict the proportions of dust emission or deposition relative to global marine dust deposition. The lines in the middle illustrate the transport direction and intensity.

1101

1102

https://doi.org/10.5194/egusphere-2025-763
Preprint. Discussion started: 6 March 2025

1103

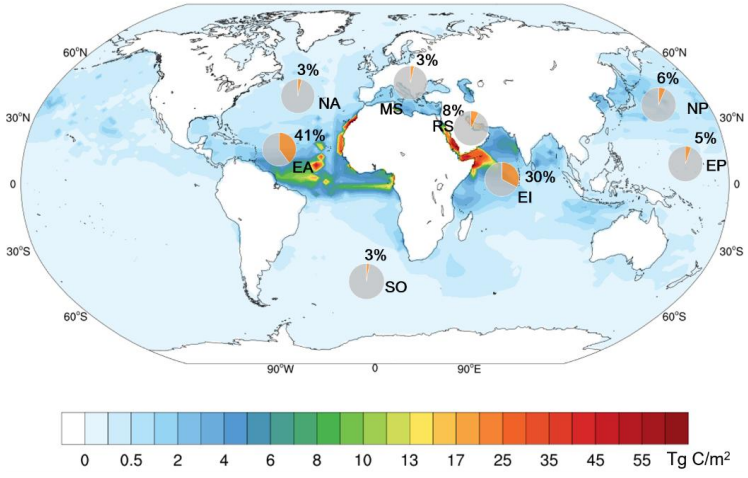

Fig. 9 The annual carbon uptake for new growth induced by dust deposition. Pie charts express the proportions of annual dust-driven carbon uptake for new growth in each ocean to global ocean

1104

1105

https://doi.org/10.5194/egusphere-2025-763
Preprint. Discussion started: 6 March 2025

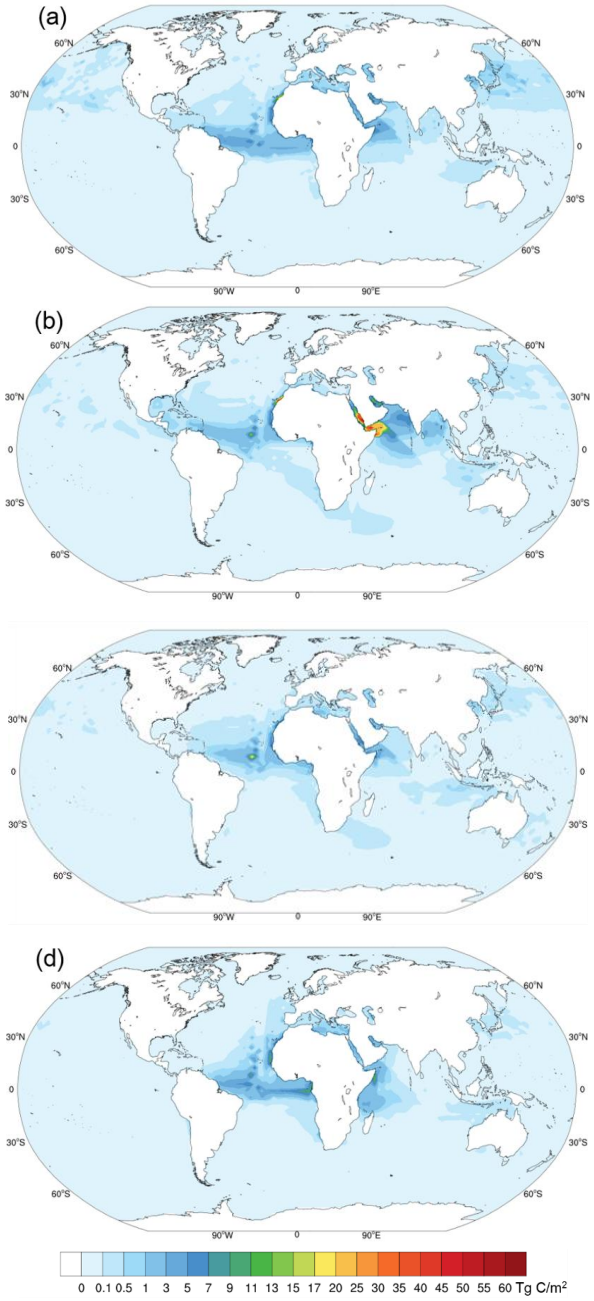

Fig. 10 The seasonal variations of marine carbon uptake for new growth to dust deposition,
(a) spring; (b) summer; (c) autumn; (d) winter.

https://doi.org/10.5194/egusphere-2025-763
Preprint. Discussion started: 6 March 2025

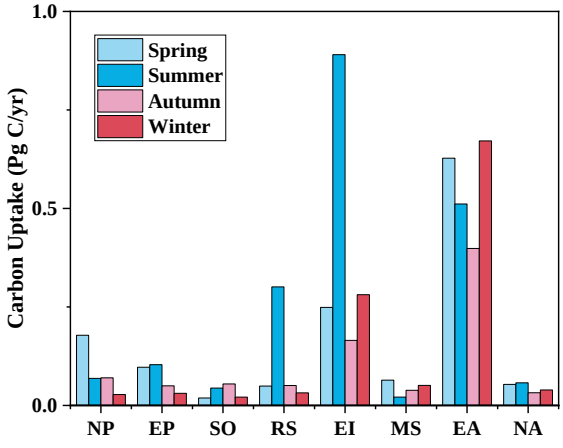

Fig. 11 Seasonal variations of carbon uptake for new growth caused by Fe supply from dust deposition over each ocean area

1106
1107

https://doi.org/10.5194/egusphere-2025-763
Preprint. Discussion started: 6 March 2025

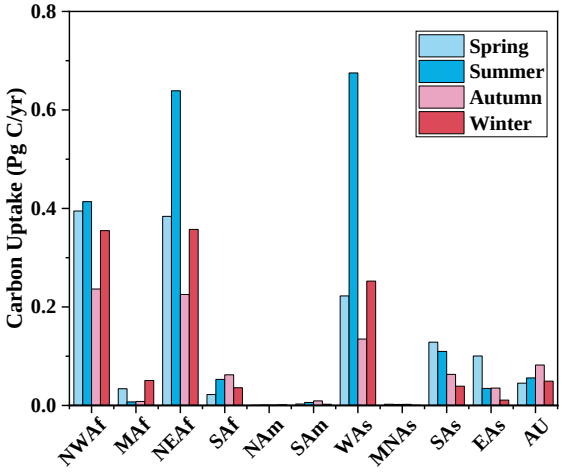

Fig. 12 Seasonal contribution of dust source regions to marine carbon uptake for new growth driven by dust deposition

1108

1109

https://doi.org/10.5194/egusphere-2025-763
Preprint. Discussion started: 6 March 2025

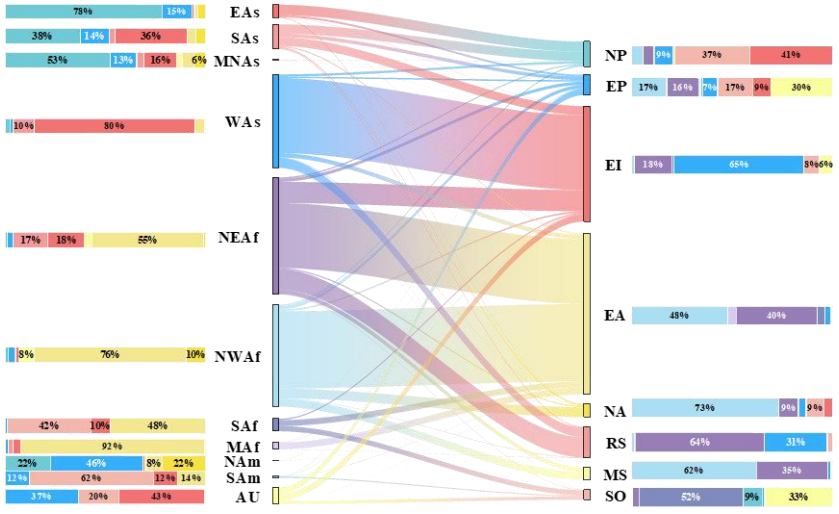

Fig. 13 The annual contribution of various dust source regions to the marine carbon uptake for new growth

The left lateral columns are the proportions of dust from each dust source to induce marine carbon uptake over each ocean, with different colors representing different oceans. The right lateral columns illustrate the contributions from various dust sources to marine carbon uptake over each ocean, different color corresponding to different dust sources. The longitudinal columns display the contribution ratios of dust sources or oceans to the total marine carbon uptake driven by dust deposition. The lines in the middle illustrate the transport direction and intensity.